NEOPLASIA
www.neoplasia.com

Volume 16 Number 7 July 2014 pp. 543–561 543

Mechanisms of Glioma Formation: Iterative Perivascular Glioma Growth and Invasion Leads to Tumor Progression, VEGF-Independent Vascularization, and Resistance to Antiangiogenic Therapy[1,2]

Gregory J. Baker*,†,‡, Viveka Nand Yadav*,†, Sebastien Motsch§,¶, Carl Koschmann*,†, Anda-Alexandra Calinescu*,†, Yohei Mineharu*,†, Sandra Ines Camelo-Piragua#, Daniel Orringer*, Serguei Bannykh, Wesley S. Nichols**, Ana C. deCarvalho††, Tom Mikkelsen††, Maria G. Castro*,† and Pedro R. Lowenstein*,†**

*Dept. of Neurosurgery, University of Michigan Medical School, Ann Arbor, MI 48109, USA; †Dept. of Cell and Developmental Biology, University of Michigan Medical School, Ann Arbor, MI 48109, USA; ‡Dept. of Molecular and Medical Pharmacology, David Geffen School of Medicine, UCLA, Los Angeles, CA 90095, USA; §Center for Scientific Computation and Mathematical Modeling, University of Maryland, College Park, MD 20742, USA; ¶School of Mathematical and Statistical Sciences, Arizona State University, Tempe, AZ 85281, USA; #Dept. of Pathology, University of Michigan, Ann Arbor, MI 48109, USA; **Dept. of Pathology and Laboratory Medicine, Cedars-Sinai Medical Center, Los Angeles, CA 90048, USA; ††Depts. of Neurology and Neurosurgery, Henry Ford Hospital, Detroit, MI 48202, USA

Abstract

As glioma cells infiltrate the brain they become associated with various microanatomic brain structures such as blood vessels, white matter tracts, and brain parenchyma. How these distinct invasion patterns coordinate tumor growth and influence clinical outcomes remain poorly understood. We have investigated how perivascular growth affects glioma growth patterning and response to antiangiogenic therapy within the highly vascularized brain. Orthotopically implanted rodent and human glioma cells are shown to commonly invade and proliferate within brain perivascular space. This form of brain tumor growth and invasion is also shown to characterize *de novo* generated endogenous mouse brain tumors, biopsies of primary human glioblastoma (GBM), and peripheral cancer metastasis to the human brain. Perivascularly invading brain tumors become vascularized by normal brain microvessels as individual glioma cells use perivascular space as a conduit for tumor invasion. Agent-based computational modeling recapitulated biological perivascular glioma growth without the need for neoangiogenesis. We tested the requirement for neoangiogenesis in perivascular glioma by treating animals with angiogenesis inhibitors bevacizumab and DC101. These inhibitors induced the expected vessel normalization, yet failed to reduce tumor growth or improve survival of mice bearing orthotopic or endogenous gliomas while exacerbating brain tumor invasion. Our results provide compelling experimental evidence in support of the recently described failure of clinically used antiangiogenics to extend the overall survival of human GBM patients.

Neoplasia (2014) 16, 543–561

Address all correspondence to: P.R. Lowenstein, MD, PhD, Richard Schneider Collegiate Professor, Professor, Department of Neurosurgery, Professor, Department of Cell and Developmental Biology, MSRB II, Room 4570, University of Michigan School of Medicine, 1150 West Medical Center Drive, Ann Arbor, MI 48109-5689, USA. E-mail: pedrol@umich.edu

[1] This article refers to supplementary materials, which are designated by Figures S1 to S7 and Movies S1 and S2 and are available online at www.neoplasia.com.

[2] This work was supported by National Institutes of Health/National Institute of Neurological Disorders and Stroke grants 1RO1-NS 054193, 1RO1-NS 061107, and 1RO1-NS082311 to P.R.L. and grants 1UO1-NS052465, 1RO1-NS 057711, and 1RO1-NS074387 to M.G.C.
Received 5 May 2014; Revised 10 June 2014; Accepted 11 June 2014

1476-5586/14
http://dx.doi.org/10.1016/j.neo.2014.06.003

"Et pour arriver a une meilleure compréhension biologique des gliomes, l'analyse des permiers débuts des processus gliomateux nous semble, pour le moment, plus importante que celle des manifestations tardives.""La croissance périvasculaire joue un grand role, dans beaucoup de gliomes, comme phénomène de croissance primitive."

"And to achieve a better biological understanding of gliomas, we believe that the analysis of the earliest stages of glioma formation, for the moment, are more important than the study of late manifestations.""Perivascular growth plays an important role in many gliomas as a phenomenon of early growth."

[Hans Joachim Scherer, 1937]

Discovery is to see what everybody else has seen, and to think what nobody else has thought.

[Albert Szent-Gyorgyi]

Introduction

Gliomas are brain cancers arising from transformed glial cells. Of all gliomas, World Health Organization grade IV glioblastoma (GBM) is the most prevalent and aggressive [1]. The diffusely invasive nature of GBM precludes its complete surgical resection, which inevitably leads to tumor recurrence and patient death within 15 to 21 months [2].

In the 1930s, Hans Joachim Scherer classified the pathology of malignant glioma growth and invasion by examining several hundred post-mortem brains of GBM patients. Scherer discovered that malignant glioma cells are preferentially associated with four distinct microanatomic structures: white matter fiber bundles, perineuronal spaces, the subpial space, and brain microvessels [3,4]. Collectively, these infiltrative tumor satellites have become known as the "secondary structures of Scherer". Despite his histopathologic observations, Scherer's work was unable to experimentally test the causes and biologic consequences of these various forms of glioma growth and invasion. More recently, others have demonstrated the occurrence of perivascular invasion in multiple experimental brain tumor models [5–7], and it has been shown that perivascular invasion increases in vascular endothelial growth factor (VEGF)–deficient glioma cells [8,9] and brain tumor xenografts treated with anti-VEGF blocking antibodies [10–13]. Clinical GBMs resistant to bevacizumab therapy also demonstrate the tendency toward perivascular invasion [14]. A better understanding of the cellular and molecular mechanisms governing the behavior of glioma growth and invasion will be required for the development of effective anti-GBM therapies.

How the behavior of individual glioma cells determines clinically relevant macroscopic tumor growth remains poorly understood. We demonstrate that orthotopic glioma cells (and glioma stem cells) from mice, rats, and humans grow perivascularly throughout tumor progression (i.e., from earliest stages to death of the host). We also observe perivascular growth in human biopsies of primary GBM, genetically induced endogenous mouse gliomas, and peripheral metastasis to the human brain. Perivascular growth causes such tumors to become autovascularized as they continuously grow along preexisting normal brain microvessels.

Agent-based computational modeling predicted that the perivascular growth pattern was independent of neoangiogenesis. We tested this prediction experimentally by blocking angiogenic signaling using antibodies targeting the VEGF-A signaling axis. VEGF-A inhibitors failed to curb progressive tumor growth and extend median survival in multiple glioma models. Our data provide a novel interpretation and understanding of perivascular brain tumor growth and invasion as a VEGF-independent mechanism of tumor vascularization, which helps explain why neoangiogenesis is dispensable for brain tumor progression and why clinical antiangiogenics fail to meaningfully extend patient survival in GBM. We propose that novel therapeutics ought to specifically target normal brain blood vessels used by perivascularly invading glioma cells to sustain progressive tumor growth.

Materials and Methods

Malignant Glioma Cell Lines and Patient-Derived GBM Samples

The mouse GL26 glioma cell line was obtained from the National Cancer Institute (Bethesda, MD). The rat CNS-1 glioma cell line was kindly provided by William Hickey (Department of Pathology, Dartmouth Medical Center, Lebanon, NH). HF2303 primary human GBM cancer stem cells were provided by Dr Tom Mikkelsen, MD (Department of Neurology, Henry Ford Hospital, Detroit, MI). The human U251 glioma cell line was provided by the National Institutes of Health (Bethesda, MD) cell bank. The human brain biopsy of mammary carcinoma metastasis was provided by Dr. W.S. Nichols, and human GBM clinical biopsies were obtained from neurosurgical patients at the University of Michigan Health System after informed patient consent (Institutional Review Board No. HUM00024610).

Animal Strains

Six- to 7-week-old C57BL/6J, Rag1^{tm1Mom}/J, and Rag1^{tm1Mom}Tg (TIE2GFP)287Sato/J mice were purchased from Jackson Laboratory (Bar Harbor, ME). RA/EGxdelCre mice were kindly provided by Angelika Bierhaus of the Department of Internal Medicine I, University of Heidelberg (Heidelberg, Germany). LEW/SsNHsd Lewis rats (200-240 g) were purchased commercially from Harlan Laboratories (Indianapolis, IN). All animal experiments were conducted in accordance with procedures approved by the University Committee on Use and Care of Animals and conformed to the policies and procedures of the Unit for Laboratory Animal Medicine at the University of Michigan.

Antibodies

The following primary antibodies were used: rat monoclonal anti-CD31/Platelet Endothelial Cell Adhesion Molecule-1 (clone: MEC13.3), Catalog No. 550274, BD Pharmingen (San Jose, CA); rabbit polyclonal anti-laminin, Catalog No. L9393, Sigma-Aldrich (St. Louis, MO); mouse monoclonal anti-human nestin (clone: 10C2), Catalog No. MAB5326, Millipore (Billerica, MA); mouse monoclonal anti–α-smooth muscle actin (SMA; clone: 1A4), Catalog No. M0851, Dako (Carpenteria, CA); humanized mouse monoclonal anti–VEGF-A (bevacizumab, Avastin), NDC: 50242-060-01, Genentech (San Francisco, CA); non-specific IgGs, Equitech-Bio Inc. (Kerrville, Tx).

Generation of De Novo Mouse GBM Using the Sleeping Beauty Transposase System

De novo GBMs were induced in mice using the Sleeping Beauty transposase system as previously described [15]. Plasmids encoding p53 shRNA and oncogenic NRAS, each flanked by Inverted Repeat/Direct Repeat sequences, were co-injected into the lateral ventricle of neonatal C57BL/6J mice along with a plasmid encoding the Sleeping Beauty transposase at a ratio of (1:1:1). Tumor formation was monitored by bioluminescence imaging due to luciferase expression by the Sleeping Beauty plasmid. Mice developing signs of tumor burden were

euthanized, and brains were harvested and processed for immunohistochemical evaluation.

Statistical Analysis

Statistical analyses were performed using GraphPad Prism 5 (GraphPad Software, Inc., La Jolla, CA). Data are reported as mean ± SEM and were examined with the statistical tests specified in each figure legend. Values were considered significant at the $P \leq .05$ level.

Results

Orthotopic Glioma Growth Is Patterned by Preexisting Brain Microvasculature

Since human malignant glioma is known to associate with distinct microanatomic brain structures, we initially sought to characterize the routes of migration used by experimental GBM cell lines from the earliest time points following their intracranial implantation until moribundity. To facilitate tumor cell visualization at single cell resolution, we genetically modified mouse (GL26) and rat (CNS-1) glioma cell lines to express mCitrine fluorescent protein, a bright and photostable mutant of yellow fluorescent protein [16]. The resultant fluorescently modified cell lines were referred to as GL26-Cit and CNS-1-Cit, respectively.

Detailed time-course analyses of intracranial GL26-Cit glioma growth from 15 minutes to 120 hours post-implantation (hpi) into the right striatum of 6- to 7-week-old syngeneic RAG1$^{-/-}$ mice revealed three distinct phases of early glioma growth over nine time points analyzed (n = 54; six mice per time point) (Figure 1, *A* and *B*). Tumors < 24 hpi were characterized by round glioma cells confined to the site of initial tumor implantation (phase I). Tumor morphology then shifted after 24 hours displaying chains of elongated glioma cells radiating away from the site of initial tumor implantation that assumed a branch-like structure (phase II). Tumor centers became increasingly dense with glioma cells >96 hours *in vivo*, resulting in a progressive widening of the tumor mass while maintaining an invasive pattern at its margins (phase III).

The growth pattern of phase II (invasive) gliomas was reminiscent of branching (i.e., bifurcating) blood vessel architecture. To test whether GL26-Cit glioma uses preexisting brain microvasculature as a microanatomic scaffold for tissue invasion, we performed fractal dimension analysis on fluorescence scanning confocal micrographs of these tumors using the box-counting algorithm of ImageJ quantitative analytical software (National Institutes of Health). This allowed us to obtain a quantitative description of tumor morphology. Tumor fractal dimension values (D values) were compared to those obtained from tumor-naïve microvasculature of two distinct transgenic mouse strains (RA/EGxdelCre and Rag1^{tm1Mom}Tg(TIE2GFP)287Sato/J), both of which express green fluorescent protein (GFP) in brain endothelium [17,18] (Figure 1*C*). Our analysis indicated that invasive gliomas (48 hpi) displayed an average D value of 1.532 ± 0.015, directly overlapping the average D value obtained from tumor-naïve mouse brain microvasculature (1.567 ± 0.024). However, preinvasive gliomas (0.25 hpi) had significantly lower average D values (1.230 ± 0.010) (Figure 1*D*). The overlap in the fractal dimension of invasive gliomas with that of tumor-naïve brain microvessels indicated that GL26-Cit assumes microvasculature-like morphology at the onset of tumor invasion. This implicated the use of preexisting brain microvessels as a scaffold for GL26-Cit glioma invasion as previously observed in mouse GL261 and rat C6 gliomas [5–7].

To substantiate our hypothesis, we implanted GL26-Cit glioma cells directly into the brain of RA/EGxdelCre mice. Fluorescence scanning confocal microscopy was used to analyze tumor morphology in brain tissue sections corresponding to the aforementioned nine time points (n = 54; six mice per time point). Not only did we find direct evidence for GL26-Cit cells using preexisting mouse brain microvessels as a scaffold for tumor invasion (Figure 1*E*), but we were also unable to find even a single example of these cells using any other known route of glioma invasion throughout the 324 brain tissue sections analyzed among 54 mice. Transcardial injections of fluorophore-conjugated lysine-fixable dextrans and immunohistochemistry with blood vessel–specific antibodies (i.e., CD31, α-SMA, and laminin) were used as alternative methods to label mouse brain microvessels (Figure S1). Both methods corroborated the presence of microvasculature-associated growth and invasion. We conclude that a strict association with preexisting brain microvasculature characterizes the intracranial invasion of GL26-Cit glioma.

To further examine GL26-Cit perivascular invasion, we performed intravital imaging with multiphoton laser scanning microscopy to examine brain tumor growth and invasion in real time through cranial windows installed over the somatosensory cortex of living RAG1$^{-/-}$ mice. Phase II brain tumors (i.e., 48 hpi) were imaged for up to 24 hours in mice maintained under anesthesia with inhaled isoflurane (n = 10). Mouse brain microvessels were visualized by intravenous tail-vein injections of rhodamine B isothiocyanate–conjugated dextrans (mw = 70 kDa) before fitting the animal on the microscope stage. Imaging experiments revealed the dynamics of early microvasculature-associated GL26-Cit invasion in real time at single-cell resolution, further demonstrating that GL26-Cit glioma invasion is guided by preexisting brain microvasculature (Figure 1*F* and Movie S1).

We next asked whether perivascular invasion occurs throughout the entire course of brain tumor progression. To assess this, we implanted low numbers of GL26-Cit cells (from 300 to as few as 10) into the striatum of RAG1$^{-/-}$ mice. Implantations of approximately 10 GL26-Cit cells extended median survival to nearly 60 days from a median survival of only 21 days at a dose of 300 cells (Figure 1*G*). Histologic analysis of GL26-Cit glioma during end-stage disease [i.e., 58 days post-implantation (dpi)] confirmed the presence of continuous perivascular invasion (Figure 1*G*).

Identification of the Microanatomic Niche Occupied by Perivascularly Invading Glioma Cells

To determine the microanatomic localization of perivascular glioma cells, we labeled GL26-Cit cells *in vitro* with electron-dense ultrasmall particles of iron oxide (USPIOs) and visualized these cells using transmission electron microscopy (TEM). TEM samples bearing gliomas corresponding to phase II (invasive) tumor growth (n = 6) were chosen to capture perivascular migration. TEM analysis consistently revealed invasive glioma cells in juxtaposition to the vascular basement membrane that covers the abluminal surface of brain microvessels (Figures 1*H* and S2). GL26-Cit tumor cells displaced normal brain tissue adjacent to the adluminal microvessel surface as they entered and migrated throughout the perivascular space, a potential space facilitating bulk diffusion of interstitial fluid throughout the brain [19–21]. The process of iterative perivascular glioma growth and invasion is illustrated in Figure 2 (*A* and *B*).

Brain Tumors of Diverse Species and Cellular Origin Exhibit Perivascular Invasion

We next evaluated whether perivascular invasion characterized brain tumors of species other than mouse. Indeed, both rat CNS-1-Cit glioma cells implanted into the striatum of syngeneic Lewis rats

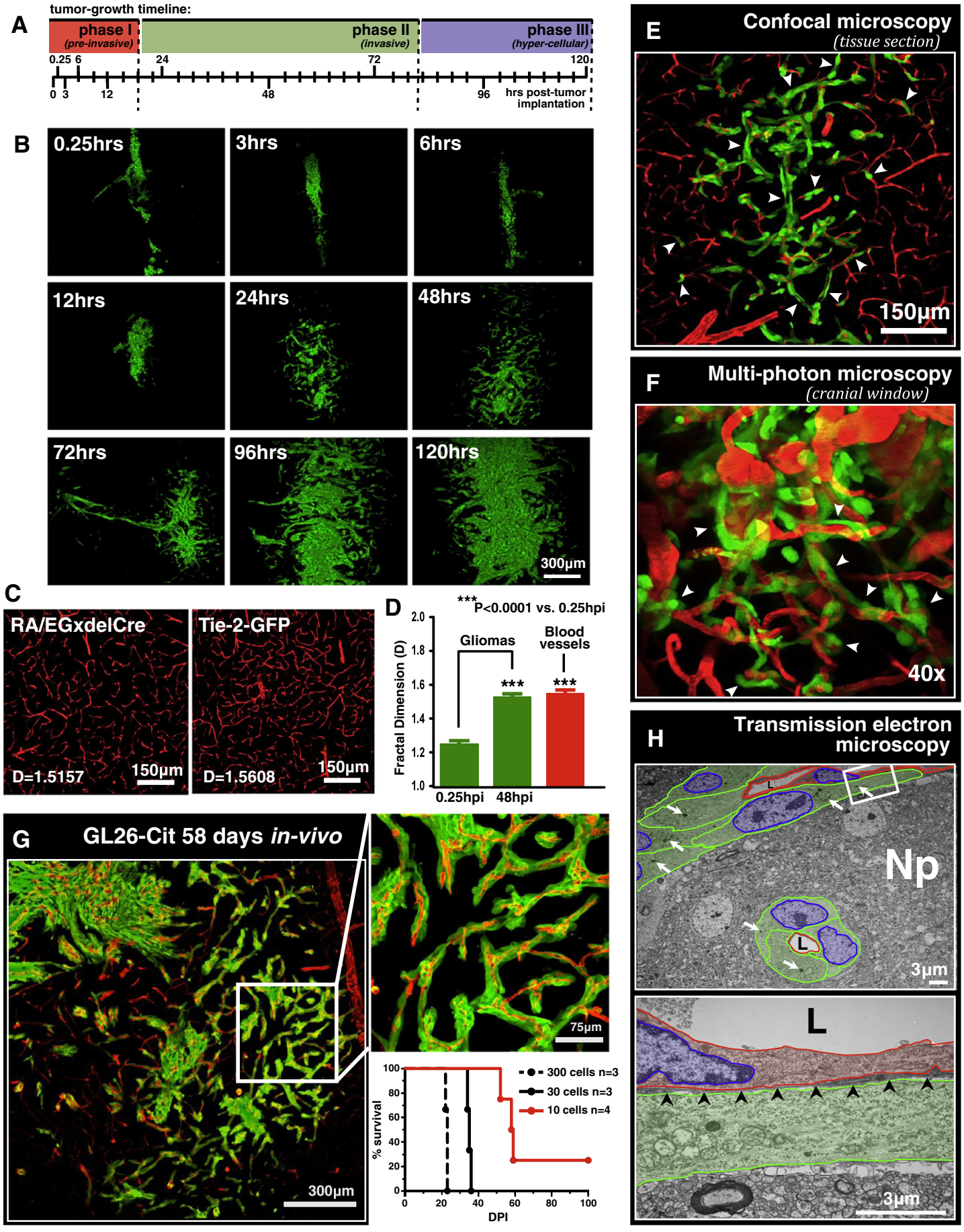
A
tumor-growth timeline:
phase I
(pre-invasive)
phase II
(invasive)
phase III
(hyper-cellular)
0.25 6
24
72
120
0 3
12
48
96
hrs post-tumor implantation
B
0.25hrs
3hrs
6hrs
12hrs
24hrs
48hrs
72hrs
96hrs
120hrs
300µm
C
RA/EGxdelCre
Tie-2-GFP
D=1.5157
150µm
D=1.5608
150µm
D
***P<0.0001 vs. 0.25hpi
Gliomas
Blood vessels
Fractal Dimension (D)
2.0
1.8
1.6
1.4
1.2
1.0
***
***
0.25hpi
48hpi
E
Confocal microscopy
(tissue section)
150µm
F
Multi-photon microscopy
(cranial window)
40x
G
GL26-Cit 58 days in-vivo
300µm
75µm
% survival
100
80
60
40
20
0
0
20
40
60
80
100
DPI
300 cells n=3
30 cells n=3
10 cells n=4
H
Transmission electron microscopy
Np
L
3µm
L
3µm

Figure 1. GL26-Cit glioma uses preexisting brain microvasculature as a scaffold for brain tumor invasion. (A) Tumor growth timeline indicating the time points analyzed over the first 120 hours of intracranial GL26-Cit glioma growth. Colored bars represent time frames corresponding to the three distinct phases of early intracranial GL26-Cit glioma growth. (B) Representative fluorescence scanning confocal micrographs of GL26-Cit glioma in the RAG1$^{-/-}$ mouse striatum imaged at the nine predetermined time points indicated in A. (C) Representative fluorescence scanning confocal micrographs of mouse brain microvessels from RA/EGxdelCre (left) and Rag1^{tm1Mom}Tg (TIE2GFP)287Sato/J (i.e., Tie-2-GFP) (right) mice used to determine the fractal dimension of normal mouse brain microvasculature. Fractal dimension values (*D* values) for each micrograph are shown. (D) Average *D* values of gliomas from RAG1$^{-/-}$ mice at 0.25 and 48 hpi ($n = 6$ mice per group) compared to the average *D* value of brain microvasculature from the two GFP^{+} mouse strains represented in C ($n = 8$; four mice per strain with five distinct striatal regions imaged per mouse). ***$P < .0001$ *versus* tumors 0.25 hpi; one-way analysis of variance followed by Tukey post-test. Data represent the mean ± SEM. (E) Fluorescence scanning confocal micrograph of GL26-Cit glioma 48 hpi into the RA/EGxdelCre mouse striatum. GFP^{+} mouse brain microvessels have been pseudocolored red. White arrowheads point to several examples of microvasculature-associated glioma invasion. (F) Intravital multiphoton micrograph of GL26-Cit glioma imaged through an intracranial window 120 hpi into the somatosensory cortex of the RAG1$^{-/-}$ mouse brain (imaging depth = 129 μm). Mouse brain microvasculature was labeled intraluminally by tail-vein injection of rhodamine B isothiocyanate–conjugated dextran (mw = 70 kDa) before imaging. White arrowheads point to numerous examples of microvasculature-associated tumor invasion. (G) GL26-Cit after 58 days post-tumor implantation into the RAG1$^{-/-}$ mouse brain shown at low (left) and high (right) magnification. Kaplan-Meier survival analysis (lower right) demonstrates that initial injections of low numbers of glioma cells extend animal survival to study late-stage tumor invasion. (H) TEM at low power (top image) showing longitudinal and transverse capillary segments (pseudocolored red) enveloped by perivascularly invading GL26-Cit glioma cells (cytoplasm, green; nuclei, blue) 48 hpi in the RAG1$^{-/-}$ mouse brain. Tumor cells displace the immediately surrounding neuropil as they enter the perivascular space. White arrows indicate USPIOs used to label tumor cells *in vitro* before implantation. Higher magnification image of the area outlined by the white box is shown below. Black arrowheads in lower micrograph point to the vascular basement membrane covering the adluminal surface of the vascular endothelium. L, vessel lumen.

($n = 6$; 3 rats per time point) and human U251 glioma cells implanted into the striatum of NU/J (i.e., nude) mice [22] ($n = 5$) used brain microvasculature as a scaffold for tumor invasion (Figure 3, *A* and *B*).

Transformed glial cells with stem cell-like properties are thought to be important contributors to clinical brain tumor initiation and progression [23]. We therefore wished to see if perivascular invasion characterized the behavior of bona fide GBM cancer stem cells. To test this, we used a patient-derived sample of primary human GBM cancer stem cells, referred to as HF2303 [24]. These cells form neurospheres when grown under serum-free conditions in the presence of human epidermal growth factor and human basic fibroblast growth factor. HF2303 cells have previously been shown to 1) express the neural stem cell markers Sox2, Musashi-1, and nestin; 2) phenocopy the original patient-derived tumor when orthotopically xenografted into immunocompromised rodents; 3) differentiate into both glial and mesenchymal cell lineages when grown intracranially [24]. HF2303 cells implanted into the striatum of RAG1$^{-/-}$ mice ($n = 15$) overtly demonstrated perivascular-associated invasion that persisted to the moribund state ~ 143 dpi (Figure 3*C*). This result indicated that perivascular invasion may underlie the invasion of clinical GBM cancer stem–like cells. We conclude that perivascular invasion is a common mechanism of orthotopic GBM invasion.

Brain microvasculature has been proposed as the "soil" in Paget's "seed and soil" hypothesis of metastasis formation [25,26]. We therefore wished to determine whether perivascular invasion also characterizes peripheral metastasis to the brain. Histologic examination of hematoxylin and eosin–stained tissue biopsies from a human patient with mammary carcinoma metastasis to the brain revealed extensive perivascular invasion at the infiltrative tumor margin (Figure 3*D*). This finding corroborates the notion of brain microvasculature as "soil" in brain metastasis and demonstrates that even peripheral cancers preferentially use preexisting microvessels as a scaffold for tissue invasion upon entering the brain.

De Novo Endogenous Mouse GBM and Clinical GBM Biopsies Exhibit Perivascular Invasion

We next wished to test whether perivascular invasion also occurs in endogenous brain tumors. To test this, we generated *de novo* mouse GBMs by co-injecting plasmids encoding p53 shRNA and oncogenic NRAS, each flanked by IR/DR sequences, along with a plasmid encoding the Sleeping Beauty transposase at a ratio of 1:1:1 into the lateral ventricle of neonatal C57BL/6J mice. Resultant GBMs were positive for the neural precursor marker, nestin, which was used to identify tumor cells. Co-immunolabeling with anti-nestin and anti–Von Willebrand factor antibodies was used to test the association of endogenous GBM cells with brain microvessels. Invasive nestin^{+} tumor cells at the infiltrative tumor margins were extensively associated with preexisting microvasculature (Figure 4*A*). We conclude that perivascular invasion characterizes the invasion of tumor cells arising *de novo* from brain-resident cells and also rules out the notion that perivascular invasion is an artifact of orthotopic brain tumor implantation.

The clinical relevance of perivascular invasion rests upon whether this phenomenon also occurs in human GBM. We therefore wished to test whether human GBM clinical biopsies would also reveal evidence of perivascular invasion. Human GBM patient biopsies were examined by a clinical neuropathologist blinded to the location of each sample. Biopsies determined to contain both glioma and normal tissue were assumed to represent the zone of transition between these two tissue types (i.e., the infiltrative tumor margin). These biopsies were then chosen for immunohistochemical analysis in our laboratory. Biopsy tissue contained cells immunoreactive for Vimentin (a marker of brain progenitor cells) and Von Willebrand factor (a marker of blood vessels). Co-immunolabeling with these two antibodies revealed the presence of perivascular-associated Vimentin^{+} tumor cells at the transition zone between neoplastic and normal tissues (Figure 4*B*). This important finding substantiates perivascular tissue invasion as a clinically relevant mechanism of human malignant brain tumor growth.

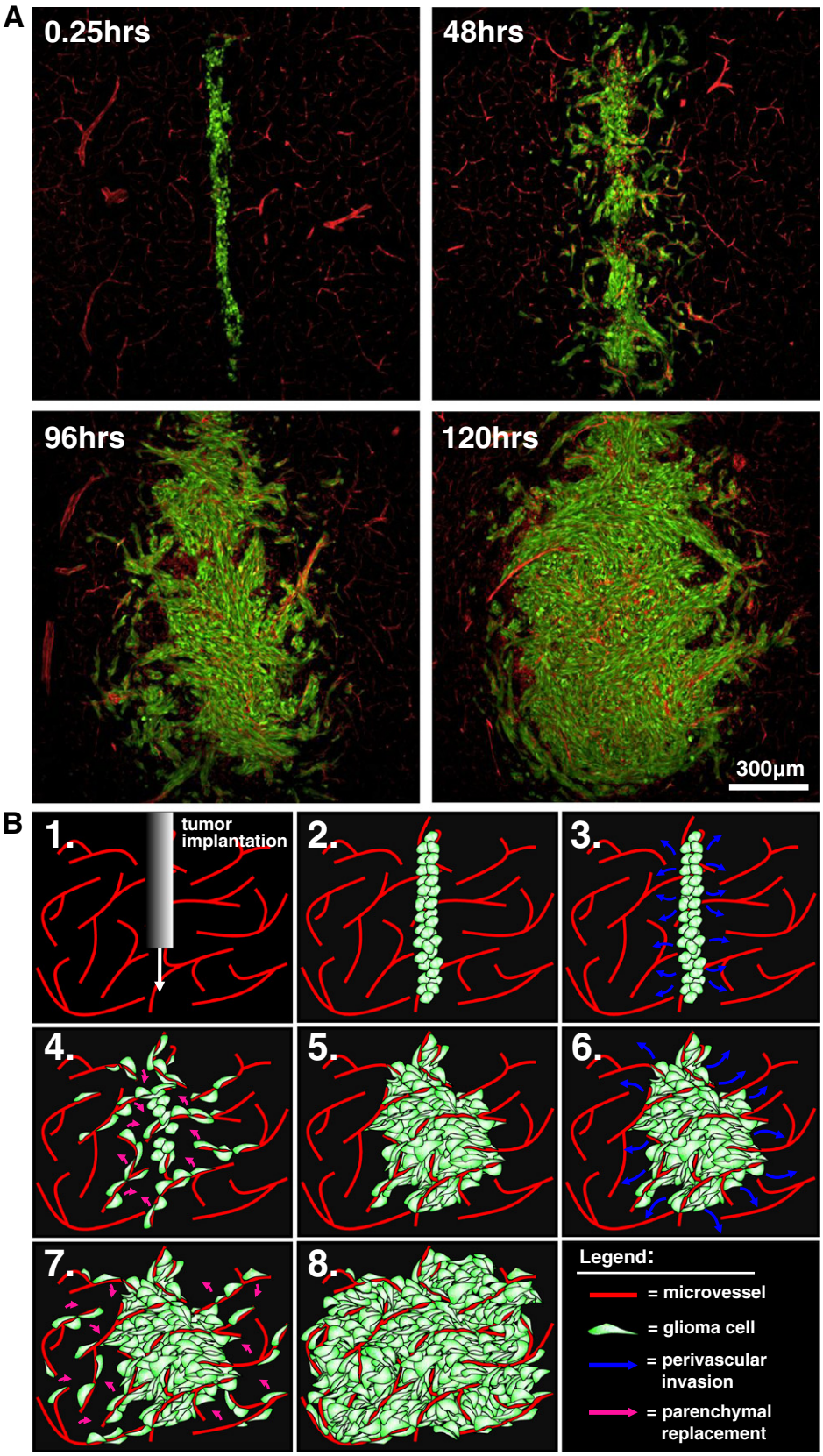

Figure 2. Perivascular invasion is an iterative growth process. (A) Scanning fluorescence confocal micrographs of GL26-Cit glioma cells from 0.25 to 120 hours in the RA/EGxdelCre mouse brain. Glioma cells are shown in green; brain microvessels are shown in red. (B) Schematic representation of the process of perivascular glioma growth and invasion beginning immediately post-tumor implantation (Step 1-2). Implanted glioma cells initially infiltrate throughout the perivascular space (Step 3-4). Cell division causes normal brain parenchyma present between adjacent microvessels to be displaced by neoplastic tissue, leaving normal brain microvessels within the tumor core (Step 4-5). Iterations of further perivascular invasion and cell division produce well-vascularized brain tumors throughout tumor growth (Steps 6-8).

Simulating Perivascular Brain Tumor Growth and Invasion

We constructed an agent-based computational model to identify the minimum number of biologic parameters required for the emergence of a perivascular pattern of brain tumor invasion. An agent-based model was chosen for its ability to simultaneously simulate the operations and interactions of multiple agents (i.e., individual glioma cells) with the underlying assumption that simple behavioral rules can generate complex behavioral patterns, leading to emergent phenomena [27]. For our purposes, we were interested in applying an agent-based model to simulate intracranial glioma behavior at the single-cell level under the assumption that glioma cells exhibit a predilection for preexisting brain microvasculature, as demonstrated by our empirical observations.

The model describes individual glioma cells by a position $(\vec{x}_i)$, a velocity $(\vec{v}_i)$, and an orientation vector $(\vec{\omega}_i)$, whose angle is denoted by θ_i [i.e., $\vec{\omega}_i = (\cos\theta_i, \sin\theta_i)$] on a two-dimensional blood vessel domain taken from real mouse brain microvessel data, which is described by a density distribution g that remains static over time (i.e., blood vessel density and position do not change over the course of the simulation). We model the displacement of each cell by a correlated random walk [28], where the transition probabilities for a single cell only depend on its last position and direction of motion. However, the displacement of glioma cells is influenced by the presence of nearby blood vessels. The motion of an individual glioma cell is fully described by the following differential equation:

$$\frac{d\vec{x}_i}{dt} = C(\vec{x}_i)(\vec{\omega}_i), \quad d\theta_i = vP_{\vec{\omega}_i}T(\nabla g(\vec{x}_i))\,dt + \sqrt{2\sigma}\;dB_t \qquad (1)$$

where the migration speed of the each glioma cell $C(\vec{x}_i)$ is a constant (i.e., $|\vec{v}_i| = C$) and is only dependent on the glioma cell's association with a blood vessel (BV) according to the following rule:

$$C(\vec{x}_i) = \begin{cases} C_0 & if\ g(\vec{x}_i) > 0 \quad (\vec{x}_i\ on\ a\ BV) \\ C_1 & if\ g(\vec{x}_i) = 0 \quad (\vec{x}_i\ not\ on\ a\ BV) \end{cases} \qquad (2)$$

Glioma cells contacting a blood vessel move slower due to adhesion effects, thus we take $C_1 > C_0$. The predilection of glioma cells for blood vessels is expressed by the velocity field $vP_{\vec{\omega}_i}T(\nabla g(\vec{x}_i))$, where the gradient $(\nabla g(\vec{x}_i))$ indicates the direction of largest increase of blood vessels. This velocity field attracts the glioma cells toward nearby blood vessels. We further denote the projection operator $P_{\vec{\omega}_i}T$ by:

$$P_{\vec{\omega}_i}T\left(\vec{F}\right) = \vec{\omega}_i T \bullet \vec{F} = \begin{pmatrix} -\sin\theta \\ \cos\theta \end{pmatrix} \bullet \vec{F} \qquad (3)$$

This projection ensures that the blood vessel attractive force only changes the direction, not the speed, of the glioma cell's migration. Finally, the term dB_t signifies the stochastic noise in the system by modeling the random perturbations exerted on glioma cells. The parameter σ in Equation (1) controls the intensity of this perturbation. Upon contacting a blood vessel (i.e., $g(\vec{x}_i) > 0$), glioma cells divide at a rate μ_b and reduce their migration speed due to adhesion effects. The daughter cell created upon cell division then begins its own independent correlated random walk. Glioma cells not in contact with a blood vessel (i.e., $g(\vec{x}_i) = 0$) eventually die at a rate μ_d, where the life expectancy of an individual glioma cell is defined as $1/\mu_d$. The key elements of the model, and its comparison to *in vivo* glioma growth, are summarized in Figure 5 (*A* and *B*). To implement the model numerically, we discretize the equation using the Euler method [29]. By optimizing only few parameters such as cell migration speed, strength of attraction to blood vessels, and cell birth and death rate, we have non-trivially recapitulated the three distinct phases of early malignant glioma growth shown empirically through our experimental data (Figure 5*C* and Movie S2). Further details on the agent-based computational model can be found in the Supplementary Materials and Methods section (Figures S3 and S4).

Perivascular Glioma Invasion Is a VEGF-Independent Mechanism of Tumor Vascularization

The growth pattern obtained from our *in silico* simulation using preexisting mouse brain microvasculature as a domain in which simulated glioma cells interact and evolve over time bore a striking resemblance to experimental data. Since our *in silico* simulation did not implement a parameter controlling tumor neoangiogenesis (i.e., the blood vessel domain remains static over the course of the simulation), the model predicted that perivascular invasion is independent of neoangiogenesis to sustain progressive tumor growth. We began to test this prediction by treating RAG1$^{-/-}$ mice bearing GL26-Cit tumors over a 144-hour time period (n = 30; two groups; five time points; three mice per group per time point) with bevacizumab, a neutralizing monoclonal antibody against VEGF-A [30], at a dose of 10 mg/kg delivered intraperitoneally (i.p.) twice weekly as previously described [31] or with non-specific control IgGs at an equivalent molar dose, route, and schedule serving as a negative control. Tumors corresponding to 24, 48, 96, 120, and 144 hours post-tumor implantation revealed no significant differences in overall tumor size or morphology between treatment groups at matched time points (Figure 6, *A*–*C*). Bevacizumab's presence in the brain was confirmed by probing mouse brain tissue sections with secondary antibodies against the humanized Fc region of bevacizumab (Figure S5). This analysis revealed large amounts of bevacizumab antibody throughout the entirety of the brain tumor and at remote distances throughout the surrounding normal brain tissue. Evidence of bevacizumab's biologic efficacy in stabilizing tumor-associated blood vessels (i.e., vessel normalization) was demonstrated by using antibodies against the vascular marker CD31. Tumor blood vessel integrity was preserved in bevacizumab-treated mice while being disrupted in the tumors of mice treated with control IgG antibodies (Figure 6*D*). These results confirmed the vasculature "normalizing" effect of bevacizumab, in which VEGF inhibitors stabilize normal vascular architecture, thus increasing vascular perfusion and reducing vasogenic edema [32–34].

We next tested the effect of bevacizumab on the survival of mice bearing perivascularly invading gliomas. Kaplan-Meier survival analysis was performed on RAG1$^{-/-}$ mice treated with either bevacizumab or control IgG. Bevacizumab treatment failed to significantly extend the overall survival of mice bearing orthotopically implanted GL26-Cit mouse glioma (Figure 6*E*) or mice bearing oncogene-induced endogenous mouse brain tumors (Figure 6*F*).

We also used DC101, a monoclonal blocking antibody targeting the mouse Vascular Endothelial Growth Factor Receptor-2 (VEGFR-2) (*flk-1/kdr*) [35] as an alternative VEGF inhibitor at a dose of 40 mg/kg delivered i.p. twice weekly as previously described [36,37] and compared its effect to control IgG (n = 30; five time points; three mice per group per time point). Treatment with DC101 also revealed no significant differences in overall GL26-Cit tumor size or

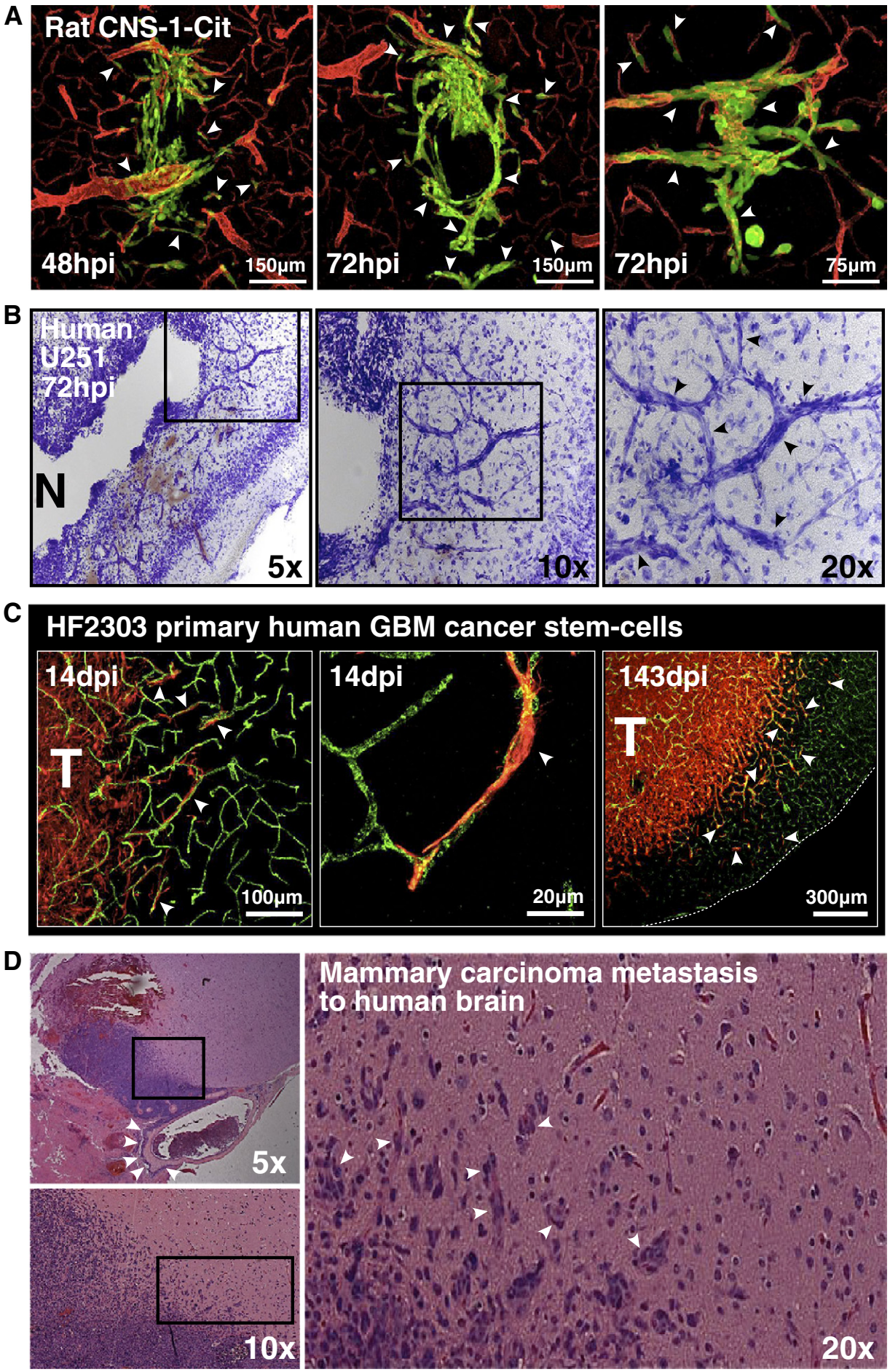
A
Rat CNS-1-Cit
48hpi
150μm
72hpi
150μm
72hpi
75μm
B
Human
U251
72hpi
N
5x
10x
20x
C
HF2303 primary human GBM cancer stem-cells
14dpi
T
100μm
14dpi
20μm
143dpi
T
300μm
D
5x
10x
Mammary carcinoma metastasis
to human brain
20x

Figure 3. Brain tumors of diverse species and cellular origin exhibit perivascular invasion. (A) Fluorescence scanning confocal micrographs of fluorescently modified CNS-1-Cit rat glioma cells in the brain of syngeneic Lewis rats after 48 hpi (left image) and 72 hpi (right two images). Brain microvasculature was immunolabeled with anti-laminin antibodies, a marker of the vascular basement membrane. White arrowheads point to distinct examples of microvasculature-associated tumor invasion. (B) Nissl staining of human U251 glioma cells in NU/J mice 72 hpi. Black boxes in each brightfield micrograph outline the field of view shown to the right at increasing magnification. Black arrows in the far right image point to tumor cell bodies heavily stained with Nissl that assume vascular morphology as they migrate away from the main tumor mass. N, tumor necrosis. (C) Fluorescence scanning confocal micrographs of HF2303 primary human GBM cancer stem cells 14 and 143 dpi into the RAG1$^{-/-}$ mouse striatum. Primary human GBM cancer stem cells are immunoreactive for the neural stem cell marker nestin. Brain microvessels have been labeled with anti-CD31 antibodies. White arrowheads indicate several examples of microvasculature-associated tumor invasion. T, bulk tumor mass. (D) Tissue biopsy from a human patient bearing mammary carcinoma metastasis to the brain. The metastatic lesion (purple) seen at low magnification (top left panel) can be seen adjacent to a large superficial blood vessel heavily infiltrated with perivascular tumor cells (white arrowheads). Higher magnification (bottom left panel) of the area outlined by the black box in the panel above reveals the invasive margin of the metastatic lesion. Largest panel to the right shows the invasive margin outlined by the black box in the bottom left image at ×20 magnification. White arrowheads point to several examples of invasive cancer cells (purple) surrounding brain microvessels (seen in red due to the presence of intraluminal red blood cells).

morphology compared to control IgG treatment at matched time points over the 144-hour analysis period (Figure 7*A*). Kaplan-Meier survival analysis performed on RAG1$^{-/-}$ mice treated with either DC101 or control IgG (n = 10; 5 mice per treatment group) confirmed the failure of anti-VEGF therapy to significantly improve the overall survival of mice bearing perivascularly invading glioma (Figure 7*B*). Further experiments using DC101 as an adjuvant therapy in combination with an efficacious anti-glioma gene therapeutic strategy [38,39] against GL26-bearing C57BL/6J mice revealed that DC101 also fails to provide additional survival benefit compared to gene therapy plus control IgG, or saline treatment alone, either before, or after, the administration of gene therapy (n = 30; 5 mice per treatment group) (Figure 7, *C* and *D*).

Conflicting evidence over whether bevacizumab can block the activity of murine VEGF-A [40–43] prompted us to treat RAG1$^{-/-}$ mice bearing primary human HF2303 GBM stem cells with the drug at the aforementioned dose, route, and schedule. Even after 54 total doses, given over 162 days of tumor growth, bevacizumab failed to significantly extend overall survival compared to treatment with control IgGs (Figure 8*A*). The brains of moribund mice were removed and photographed to document gross brain morphology before sectioning. While the brains of non-specific IgG-treated control mice exhibited extensive microvascular hemorrhage, evidence of microvascular hemorrhage was completely absent in mouse brains treated with bevacizumab (Figure 8*B*). Immunohistochemistry with human-specific anti-nestin and anti-CD31 antibodies revealed normalized tumor microvasculature deep within tumor tissue in bevacizumab-treated mice, as seen previously in bevacizumab-treated mouse GL26-Cit tumors. Conversely, control IgG–treated brain tumors revealed fragmented microvessels lacking mature microvascular architecture (Figure 8*C*). Treatment with bevacizumab also exacerbated tissue invasion (Figures 8*C* and S6). Control IgG–treated tumors grew in a nodular fashion and appeared to compress the contralateral hemisphere, while bevacizumab-treated brain tumors exhibited a more diffuse growth pattern, crossing over into the contralateral striatum without evidence of compression. These results are compatible with the beneficial effects of bevacizumab in human GBM patients (i.e., reduced intracerebral edema and improved brain function).

The phenomenon of perivascular glioma invasion, coupled with ultrastructural data indicating that glioma cells displaced normal brain tissue as they enter brain perivascular space, prompted us to quantify the average intervessel distance in the brain and the average size of glioma cells *in situ* so that we could estimate the number of glioma cells required to occupy the space between neighboring microvessels. To do so, we measured average intervessel distance in the striatum using confocal micrographs of brain tissue sections from immunolabeled C57BL/6J or GFP$^+$ endothelium from RA/EGxdelCre mice using Leica analytical software (Figure 9, *A* and *B*), which both reveal calculated average intervessel distances ($AIVD_{calc}$) of 56 μm in two dimensions. Micrographs of perivascularly invading GL26-Cit glioma cells over the first 120 hours *in vivo* were used to calculate an average tumor cell diameter (ACD_{calc}) of 21 μm (Figure 9*C*), indicating that as few as three glioma cells (or 56 μm/21 μm) are required to span the distance between adjacent microvessels. Furthermore, a sphere of mouse brain tissue 1 mm^3 is densely filled with brain microvessels (Figure 9*D*), thus perivascular invasion and high brain microvascular network density promote well-vascularized tumors early in development. On the basis of these quantitative results of brain microvessel density and the insights gained from our experimental and computational modeling of perivascular brain tumor growth, we propose a model of iterative, neoangiogenesis-independent, perivascular brain tumor growth and invasion referred to as "autovascularization" (Figure 10).

Discussion

Our investigations have elucidated how the preference of rodent malignant glioma cells and human glioma stem cells to migrate within brain perivascular space allows glioma cells to achieve diffuse brain infiltration and the formation of lethal macroscopic tumors without the need for new blood vessel formation. However, earlier literature has proposed that nascent tumors form without direct access to blood vessels and only grow to a limited volume (1 mm^3 or 1 × 10^6 cells) before necessitating access to VEGF-dependent neovascularization to rescue tumors from dormancy [5,7,44,45]. Our work shows that avascular tumor growth is impossible in the context of the brain, as a sphere of brain tissue 1 mm^3 is already densely filled with brain microvessels. This quantitative analysis also suggests that only three to six glioma cells will suffice to fill the space between two adjacent microvessels by displacing normal brain parenchyma as they invade and divide within the perivascular space. It is therefore apparent that at no time during malignant brain tumor progression is the tumor mass devoid of a blood supply, effectively precluding an avascular phase of

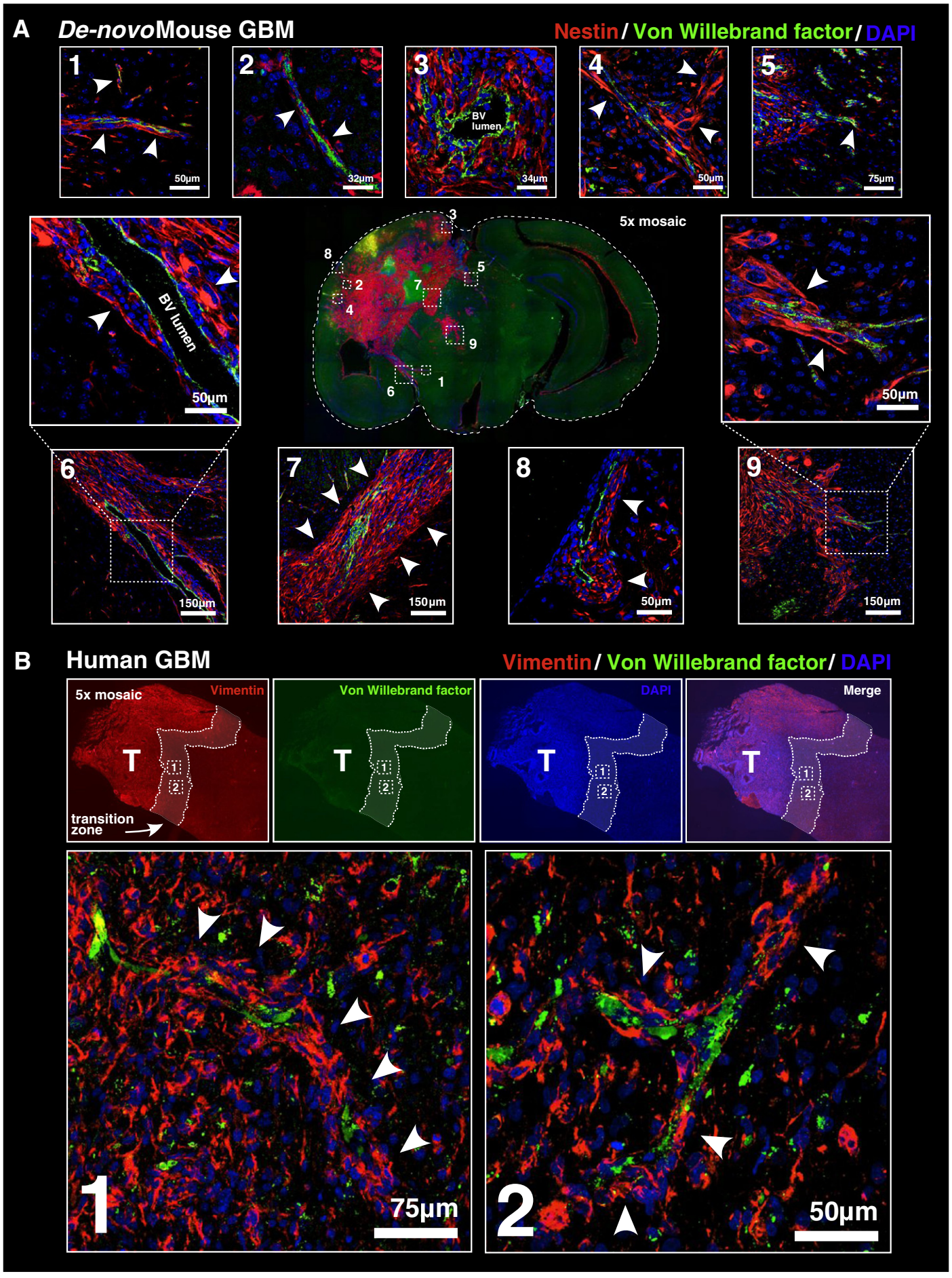
A
De-novoMouse GBM
Nestin / Von Willebrand factor / DAPI
1
50μm
2
32μm
3
BV lumen
34μm
4
50μm
5
75μm
5x mosaic
BV lumen
50μm
50μm
6
150μm
7
150μm
8
50μm
9
150μm
B
Human GBM
Vimentin / Von Willebrand factor / DAPI
5x mosaic
Vimentin
Von Willebrand factor
DAPI
Merge
T
transition zone
1
75μm
2
50μm

Figure 4. *De novo* mouse GBM and clinical GBM biopsies exhibit perivascular invasion. (A) *De novo* mouse GBM generated using the Sleeping Beauty transposase system at 60 days post-plasmid injection. At the center, a 5× mosaic epifluorescence micrograph of a coronal mouse brain tissue section is shown. Tumor cells have been labeled using anti-nestin antibodies. Brain microvasculature has been labeled with anti–Von Willebrand factor antibodies. 4',-diamidino-2-phenylindole (DAPI) has been used as a counterstain (blue). Numbered white boxes within the central epifluorescence micrograph correspond to respectively numbered higher magnification fluorescence scanning confocal micrographs surrounding it. Several examples of perivascular tissue invasion are indicated by white arrowheads. (B) Human GBM clinical biopsy. A 5× mosaic epifluorescence micrograph of a tissue biopsy immunolabeled with anti-vimentin antibodies, anti–Von Willebrand factor antibodies, and DAPI (blue) as a counterstain is shown. The zone of transition between tumor tissue (left) and normal brain (right) lies within the white dashed lines overlying each fluorescence channel. Panels below the high-magnification fluorescence scanning confocal micrographs correspond to the dashed white boxes from the epifluorescence images above. White arrowheads in each confocal micrograph point to examples of perivascular tissue invasion.

intracranial tumor growth. Indeed, microvessel density in GBM is comparable to the surrounding normal brain [46] supporting the notion that human glioma progression may proceed by autovascularization.

Perivascular invasion causes spontaneous tumor vascularization in a VEGF-independent manner by engulfing preexisting brain microvessels and replacing normal brain parenchyma over the course of tumor progression (see Figure 10). We propose the term "autovascularization" to describe this form of continuous brain tumor growth and invasion. The VEGF independence of glioma autovascularization is supported by our data showing that the use of VEGF inhibitors bevacizumab and DC101 fail to curb tumor progression or improve median survival in mice bearing human or mouse malignant glioma.

The brain perivascular compartment is a potential space between the vascular basement membrane and the immediately surrounding glia limitans, derived from [19] astrocytes which impart blood–brain barrier characteristics to the vascular endothelium. Because brain perivascular space serves as the point of entry for oxygen, glucose, and other nutrients into the brain, it is ideally suited to support the high metabolic demand of rapidly proliferating tumor cells. Perivascular tumor cells therefore benefit from the ample amounts of glucose entering the brain for use in the glycolytic pathway, the preferred metabolic pathway of transformed cells according to the Warburg effect [47]. Indeed, it has recently been shown that anaerobic glycolysis is favored by brain tumor initiating cells, cells thought responsible for initiating and maintaining progressive tumor growth in human glioma [48]. The basement membrane covering the adluminal microvessel surface is rich in extracellular matrix proteins such as laminin, fibronectin, and vitronectin. These highly glycosylated extracellular matrix proteins are binding partners in integrin-mediated cellular adhesion, promote cellular migration, and activate pro-survival signaling pathways [49]. For these reasons, the preference of invasive glioma cells for brain perivascular space may serve to 1) provide an oxygen, glucose, and nutrient-rich microenvironment ideal for the survival of highly metabolic neoplastic tissue and 2) promote cell adhesion/migration and stimulate pro-survival pathways in cancer cells.

Though the literature regarding the inhibitory effect of bevacizumab against mouse VEGF-A (mVEGF-A) is contradictory, the original developers of A.4.6.1, a mouse anti-VEGF monoclonal antibody subsequently humanized and branded as bevacizumab (Avastin) [50], maintain that the antibody has low affinity for mVEGF-A. However, various research groups have shown the biologic efficacy of bevacizumab against mVEGF-A [41–43], and our own results showing brain tumor vessel normalization are all consistent with the claim that bevacizumab indeed blocks mVEGF-A. A dose of 10 mg/kg delivered i.p. every 3 days normalized tumor-associated mouse brain microvessel architecture in the murine GL26-Cit glioma model. This effect was comparable to that demonstrated by bevacizumab treatment of HF2303 cells, primary human GBM cancer stem cells, suggesting that bevacizumab in fact exerts a biologic effect on both human- and mouse-derived VEGF-A *in vivo.*

Blood–brain barrier compromise leads to intracerebral vasogenic edema and neurologic symptoms in GBM [51]. VEGF inhibitors, such as bevacizumab, are therefore thought to improve quality of life by stabilizing normal brain microvessel structure and reducing brain edema [32,33]. Our experimental data with HF2303 human glioma-derived stem cells treated with bevacizumab demonstrate the normalizing effect on tumor-associated microvasculature in a model of primary human GBM stem cells; these experiments also demonstrate the substantial increase in the invasion of human glioma stem cells caused by bevacizumab [11,52]. We therefore conclude that bevacizumab-mediated symptom reduction likely involves 1) a reduction in intracerebral vasogenic edema by stabilizing tumor-associated brain microvessels and 2) a lessening of intracerebral compression of eloquent brain regions by exacerbating diffuse tumor invasion. This suggests that VEGF inhibitors, despite potential beneficial effects, may be deleterious to patients by promoting widespread tumor invasion. The recently reported failure of bevacizumab to prolong patient life in randomized human glioma clinical trials [53,54] is compatible with our results. Indeed, our data provide a basic biological framework potentially underlying these clinical results. It remains to be examined whether increased invasion caused by bevacizumab is dependent on basal levels of tumor-derived VEGF secretion or the intrinsic tendency for glioma cells to invade perivascularly [12,55,56].

We have not overlooked the fact that malignant glioma cells may use other growth pathways in addition to, or in lieu of, the perivascular space. However, we suspect that all forms of malignant glioma invasion may preclude the requirement for new blood vessel formation to support tumor progression. In the future, we aim to further examine and catalogue the diverse invasion patterns of malignant glioma cells. By identifying the various ways in which malignant glioma cells invade the brain, combinatorial therapeutics that block multiple migration pathways in order to effectively treat human malignant brain tumors may be developed. We propose that new therapies directly targeting the perivascular space and normal brain blood vessels that sustain glioma growth and invasion may prove efficacious targets in the treatment of malignant glioma by curbing diffuse tumor infiltration throughout the interconnected microvessel network. Cytotoxic therapies targeting tumor-associated

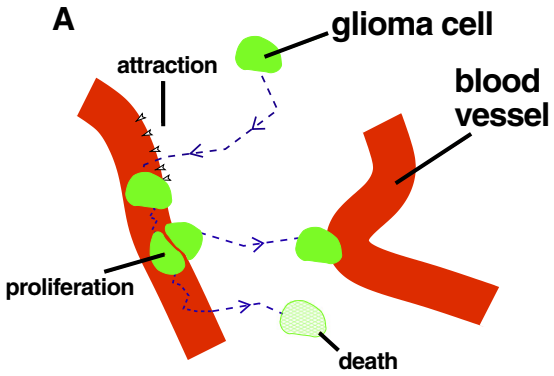

B

Parameter	Symbol	Value
Cell speed	C	10 $\mu m/h$
Cell speed on BV	C_0	1 $\mu m/h$
Noise	σ	0.25 h^{-1}
Attraction to BV	ν	20 $\mu m/h/bv$
Birth rate	μ_b	1/30 h^{-1}
Death rate	μ_d	1/100 h^{-1}

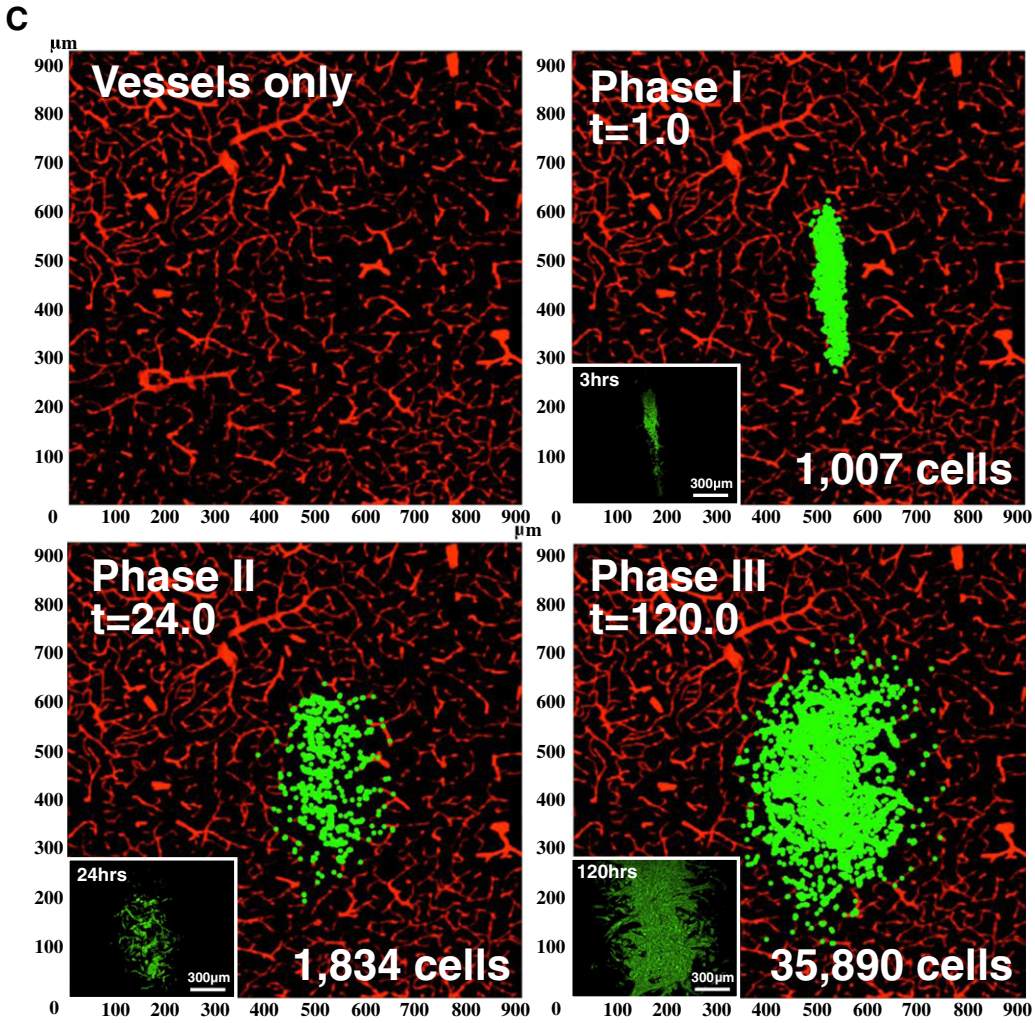

Figure 5. *In silico* computational modeling mimics perivascular brain tumor growth. (A) Schematic representation of an agent-based computational model describing perivascular brain tumor growth and invasion. Individual glioma cells move toward nearby blood vessels under the influence of a velocity field $vP\vec{\omega}_i T(\nabla g(\vec{x}_i))$ that mimics the predilection of glioma cells for blood vessels (an underlying assumption of the model). Cells move by a correlated random walk with constant speed toward nearby blood vessels. Once tumor cells make contact with a vessel, they slow their migration speed and proliferate at a rate μ_b. Tumor cells not associated with a blood vessel eventually undergo cell death at a rate μ_d and have an average life expectancy of $1/\mu_d$. BV, blood vessel. (B) A table summarizing the parameters used in the agent-based model. The respective symbols and optimal values are indicated for each parameter. (C) Representative snapshots of simulated brain tumors corresponding to the three phases of early perivascular tumor growth. The microvasculature domain (vessels only) has been taken from a fluorescence scanning confocal micrograph of RA/EGxdelCre mouse brain microvessels. The simulated tumor initially consists of 1×10^3 cells centered with the microvasculature domain at $t = 0$, simulating preinvasive phase I glioma soon after implantation (top right panel). Tumor cells then begin to migrate toward nearby microvessels resulting in a strong correlation between the density of tumor cells and blood vessels, causing the characteristic branch-like morphology of phase II glioma (bottom left panel). Tumor cells making contact with a blood vessel rapidly proliferate and fill the gaps between adjacent blood vessels as the total number of cells grows exponentially. As a result, the tumor center widens and becomes hypercellular while maintaining extensive microvascular contact at the tumor borders in a fashion that mimics phase III glioma (bottom right panel).

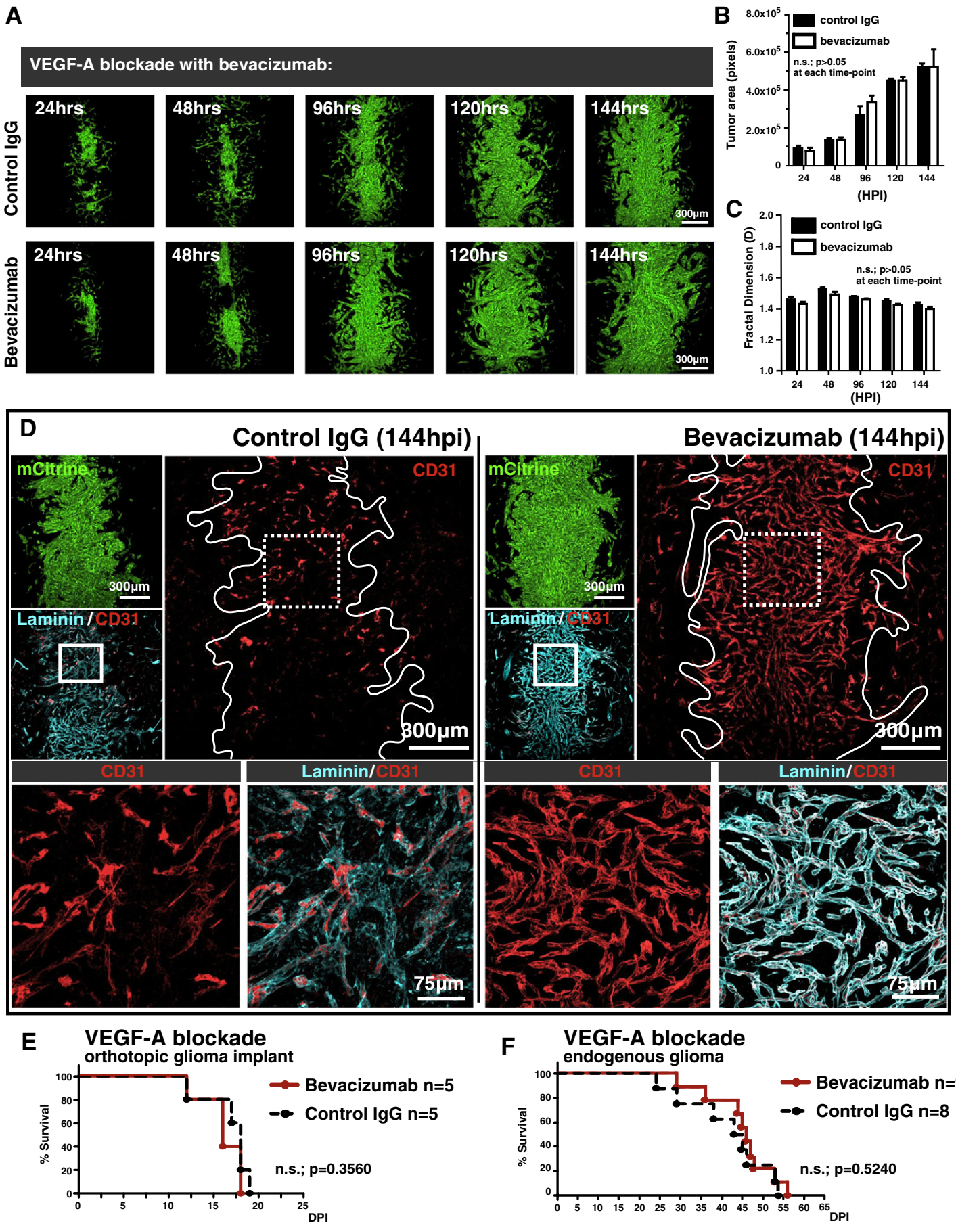
A
VEGF-A blockade with bevacizumab:
Control IgG
Bevacizumab
24hrs
48hrs
96hrs
120hrs
144hrs
300μm
B
Tumor area (pixels)
control IgG
bevacizumab
n.s.; p>0.05
at each time-point
(HPI)
C
Fractal Dimension (D)
control IgG
bevacizumab
n.s.; p>0.05
at each time-point
(HPI)
D
Control IgG (144hpi)
Bevacizumab (144hpi)
mCitrine
CD31
Laminin/CD31
300μm
75μm
E
VEGF-A blockade
orthotopic glioma implant
Bevacizumab n=5
Control IgG n=5
% Survival
DPI
n.s.; p=0.3560
F
VEGF-A blockade
endogenous glioma
Bevacizumab n=9
Control IgG n=8
% Survival
DPI
n.s.; p=0.5240

Figure 6. Perivascular glioma invasion obviates the requirement for tumor neoangiogenesis to support continual intracranial growth. (A) Representative fluorescence scanning confocal micrographs of GL26-Cit glioma over the initial 144 hpi in the RAG1$^{-/-}$ mouse brain. Mice were treated with non-specific control IgG (top row) or the VEGF-A blocking antibody bevacizumab (bottom row). (B and C) Quantification of time point–matched tumors ($n = 30$; three tumors per group per time point) reveals no significant difference in overall tumor size as measured by the average tumor area in pixels (B) or morphology as measured by tumor fractal dimension (C) between control IgG– and bevacizumab-treated mice over the 144-hour analysis period. The P value between treatment groups was >.05 at each time point analyzed by two-way analysis of variance followed by Bonferroni post-tests. (D) Immunohistochemistry on GL26-Cit bearing mouse brain tissue sections labeled with the vascular markers CD31 and laminin (cyan) after 144 hours of treatment with control IgG (left) or bevacizumab (right). Solid white tumor outlines in the CD31 channels circumscribe tumor-associated microvasculature and reveal the vessel "normalization" effect in the bevacizumab treatment group. Dashed white boxes outline the area imaged at higher magnification in the two images below each treatment group, further revealing the anatomic detail of vessel preservation in the bevacizumab-treated group. (E) Kaplan-Meier survival analysis of RAG1$^{-/-}$ mice bearing GL26-Cit glioma treated with bevacizumab ($n = 5$) or control IgG ($n = 5$). Mantel-Cox log-rank test detected no significant survival difference between the bevacizumab and control IgG treatment groups ($P = .3560$). (F) Kaplan-Meier survival analysis of RAG1$^{-/-}$ mice bearing endogenous brain tumors generated *de novo* using the Sleeping Beauty transposase system treated with bevacizumab ($n = 9$) or control IgG ($n = 8$). Mantel-Cox log-rank test detected no significant survival difference between the bevacizumab and control IgG treatment groups ($P = .5240$).

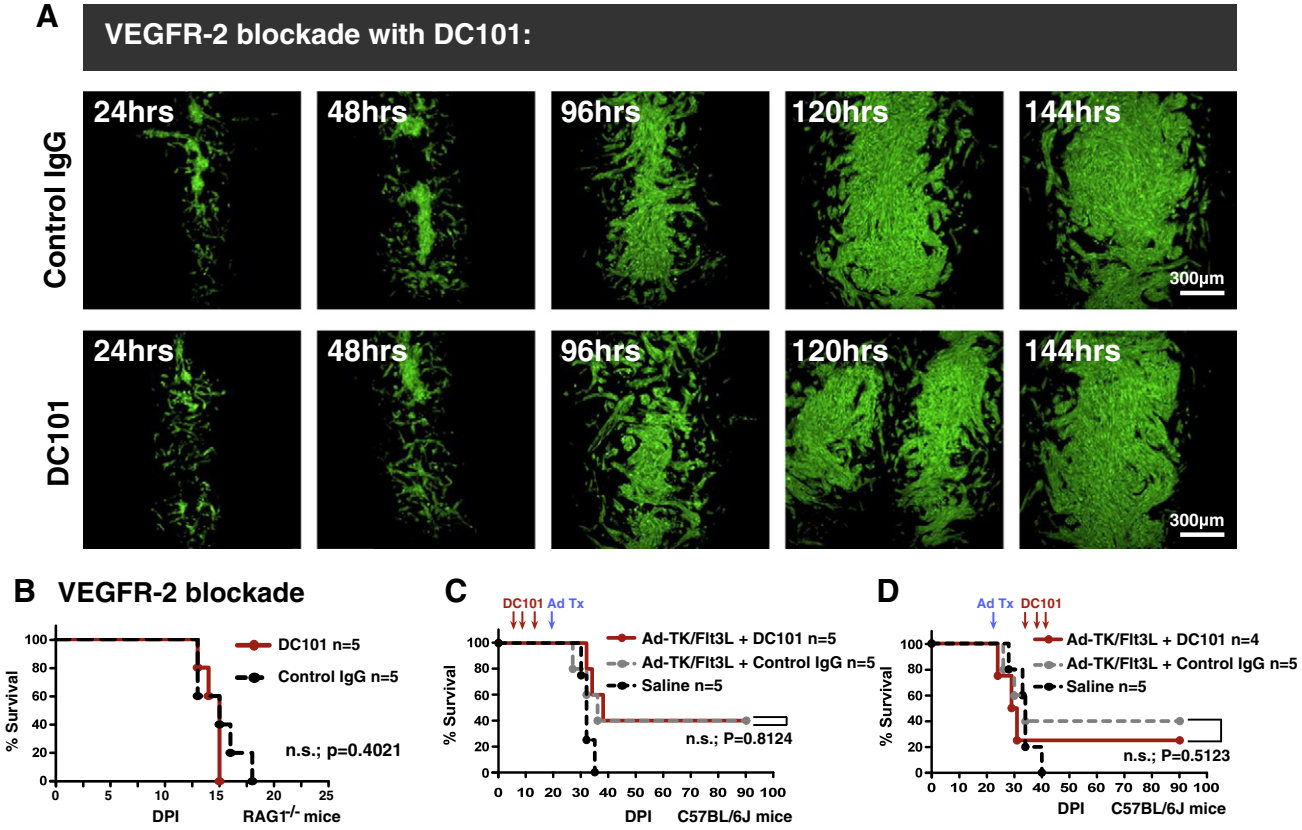

Figure 7. VEGFR-2 blockade with DC101 fails to inhibit tumor growth over 144 hours *in vivo* or improve survival alone, or as adjuvant therapy. (A) Representative fluorescence scanning confocal micrographs of GL26-Cit tumors in RAG1$^{-/-}$ mice treated with control IgG (top row) or DC101 (bottom row) at a dose of 40 mg/kg delivered i.p. twice weekly over 144 hours ($n = 30$; three mice per time point per treatment group). No discernable difference in tumor size or morphology is noted at each time point analyzed. (B) Kaplan-Meier survival analysis comparing C57BL/6J mice bearing GL26 gliomas treated with DC101 or control IgG administered three times (red arrows) before (B), or after (C), treatment with Ad-TK/Ad-Flt3L adenovirally mediated cytotoxic gene therapy. Saline treatment alone was used as a negative control. Mantel-Cox log-rank test detected no significant survival difference between Ad-TK/Ad-Flt3L plus DC101 and Ad-TK/Ad-Flt3L plus control IgG treatment either before ($P = .8124$) or after ($P = .5123$) treatment with Ad-TK/Ad-Flt3L.

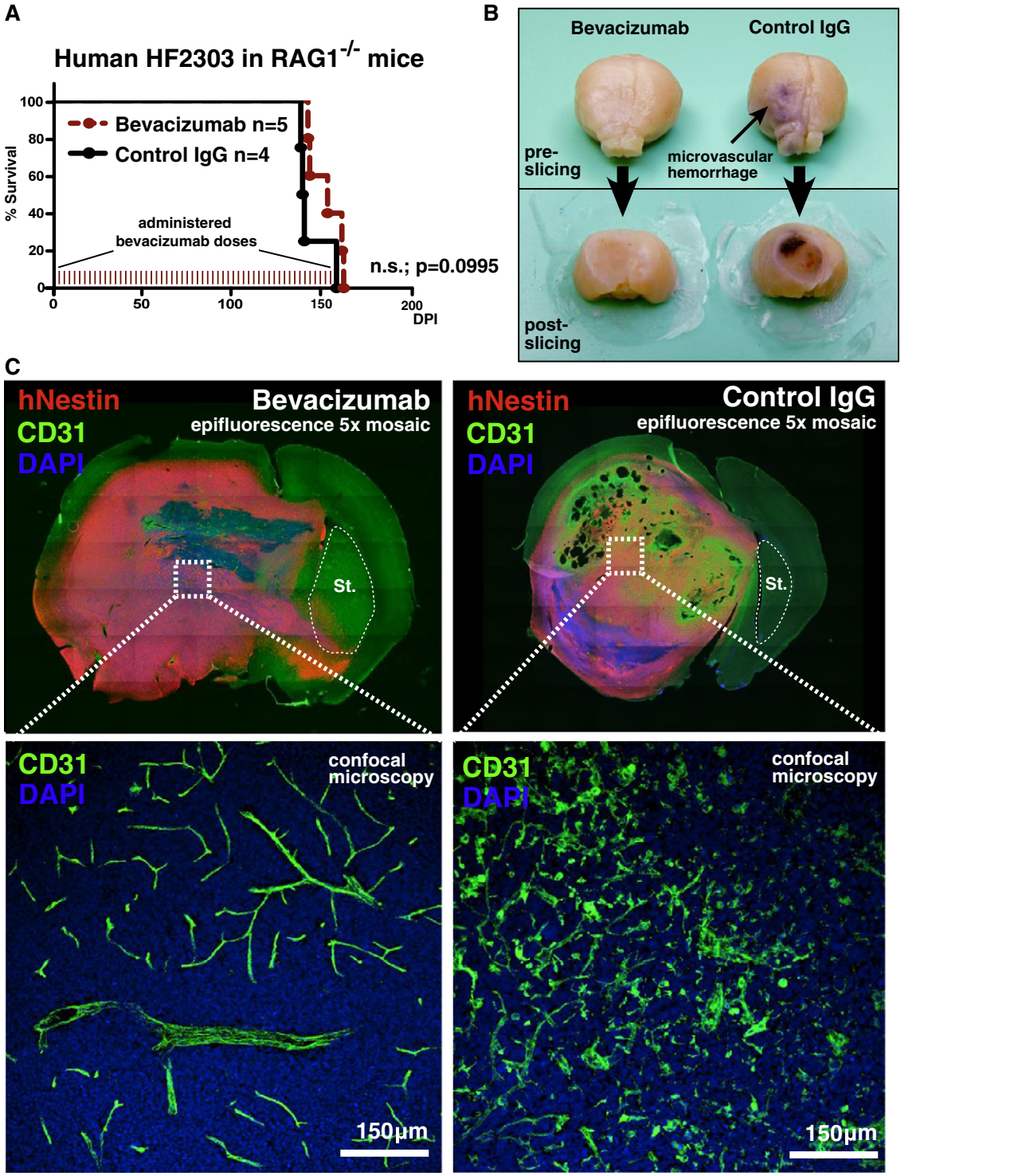

Figure 8. Bevacizumab does not significantly improve the survival of RAG1 $^{-/-}$ mice bearing HF2303 primary human GBM stem cells. (A) Kaplan-Meier survival analysis of RAG1 $^{-/-}$ mice bearing human HF2303 GBM stem cells treated with bevacizumab or non-specific control IgG. Mantel-Cox log-rank test detected no significant survival difference between the bevacizumab and control IgG treatment groups (P =.0995). Each tick denotes 1 of the 54 total doses of bevacizumab administered throughout the study. n.s., not significant. (B) Representative photographs of gross brain morphology from moribund RAG1 $^{-/-}$ mice treated with bevacizumab (left) or control IgG (right) both before (top images) and after (bottom images) sectioning. Note the extensive microvascular hemorrhage associated with tumor neoangiogenesis in the control IgG treatment group, which is completely absent in bevacizumab-treated brain tumors. (C) 5 × mosaic epifluorescence micrographs of coronal brain tissue sections from the mouse brains shown in B. Sections have been immunolabeled with human-specific anti-nestin antibodies to label tumor cells, anti-CD31 antibodies to label brain microvasculature, and DAPI as a counterstain to label nuclei (blue). Note that the contralateral striatum in the control IgG treatment group (denoted as St.; dashed white outlines) appears compressed, presumably due to nodular tumor growth while bevacizumab treatment induces massive invasion into the contralateral hemisphere. Dashed white boxes in the respective images correspond to high-magnification fluorescence scanning confocal micrographs shown below. Normalized tumor vascular is specifically seen in bevacizumab-treated human HF2303 tumors, while control IgG–treated brain tumors are characterized by extensive microvessel fragmentation.

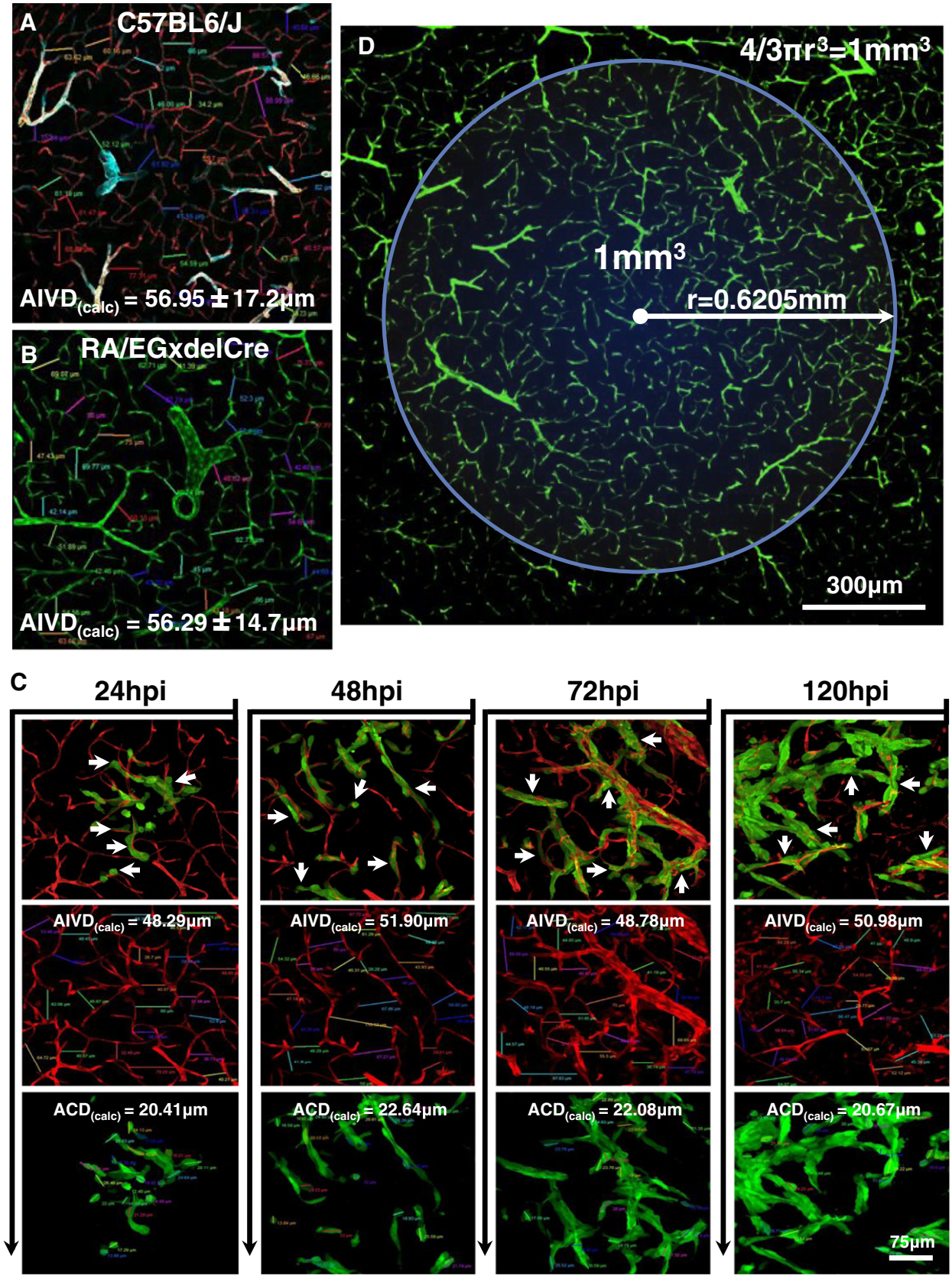

Figure 9. Quantification of brain microvascular network density. (A) Microvessels within the C57BL/6J tumor-naïve striatum were immunolabeled with anti-CD31, anti-laminin (cyan), and anti–α-SMA vascular markers and display a calculated average intervessel distance ($AIVD_{calc}$) of 56.95 ± 17.2 μm. (B) Microvessels within the RA/EGxdelCre tumor-naïve striatum showing an $AIVD_{calc}$ of 56.29 ± 14.7 μm, in good agreement with the values obtained in A, indicating a low degree of variability in this parameter between different mouse strains. (C) Analysis of invasive GL26-Cit glioma cells at various time points at the infiltrative tumor margin within the RA/EGxdelCre mouse striatum (microvessels shown in red). Composite images (top row) show close vascular contacts made by individual tumor cells at each time point analyzed (white

arrows). Individual fluorescence channels (middle and bottom rows) show $AIVD_{calc}$ and calculated average tumor cell diameters (ACD_{calc}) for the respective micrographs. Overall averages for $AIVD_{calc}$ and ACD_{calc} were determined to be 49.99 and 21.45 μm, respectively. (D) Low-magnification fluorescence scanning confocal micrograph of striatal microvasculature in the tumor-naïve RA/EGxdelCre brain. The blue circle illustrates the large number of brain microvessels present within a sphere of 1 mm^3, a volume below which many solid tumors are thought togrow avascularly (here, we assume that microvessel density does not change significantly $\pm$ 1 mm in the Z direction). The radius of the circle has been calculated by solving for $\left[r = \sqrt[3]{(3\,\mathrm{mm}^3/4)}\right]$ in the equation for the volume of a sphere measuring 1 mm^3 (upper right corner). The white arrow indicates the radius (r = 0.6205 mm) of the 1-mm^3 sphere. The combination of high microvessel density and perivascular tumor invasion is predicted to preclude an avascular phase of brain tumor growth.

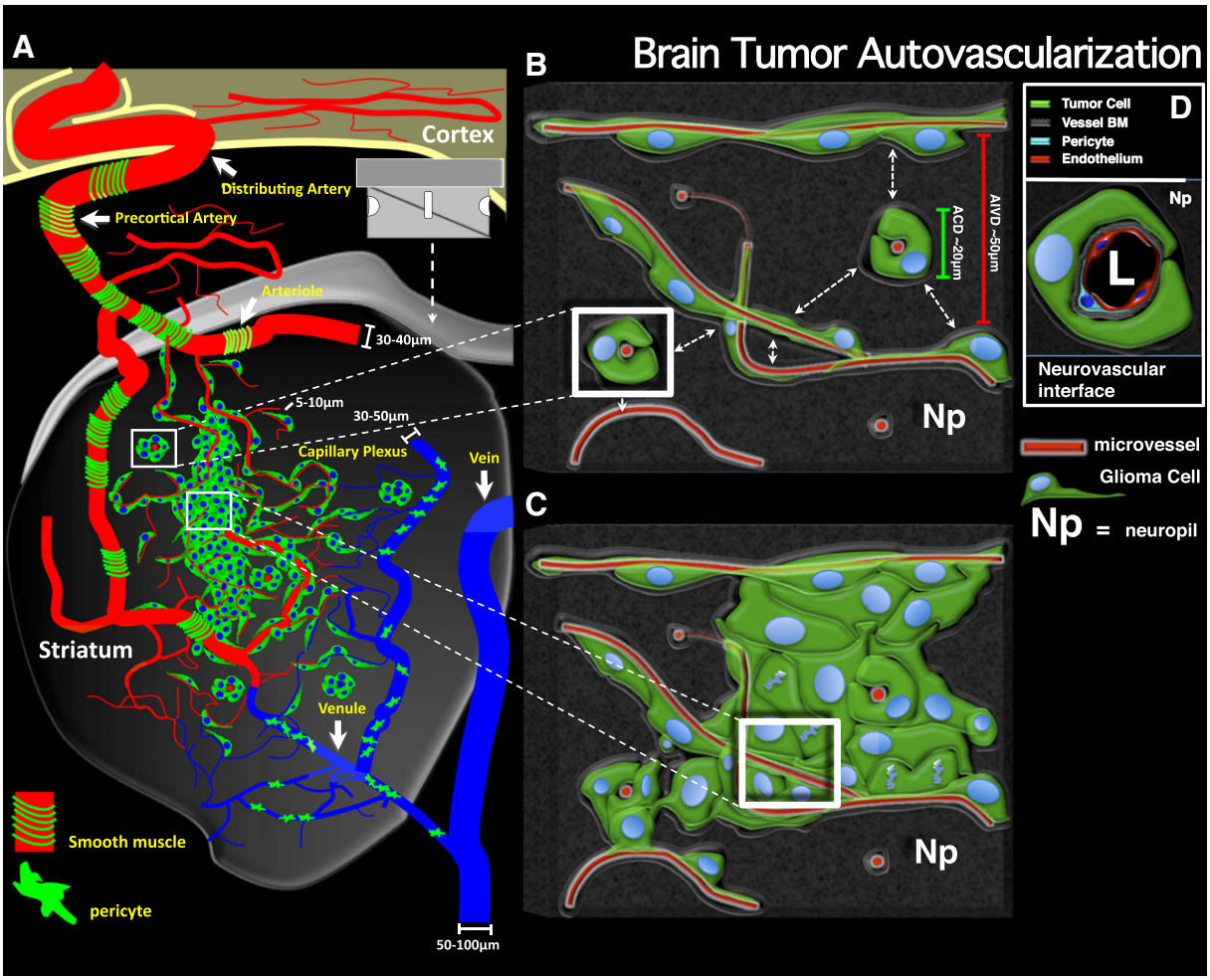

Figure 10. Brain tumor autovascularization. (A) Schematic representation of a coronally sectioned mouse brain revealing perivascular glioma growth and invasion within the striatum. Individual glioma cells are shown in green with blue nuclei. The tumor mass is vascularized with preexisting brain microvessels due to invasive glioma cells entering perivascular channels at the tumor border. Brain microvasculature is classified as arterial or venule (blue). Arterials are further characterized by the presence of smooth muscle (green bands) around larger diameter vessels, while the venous system is covered by patchwork pericytes (green amoeboid cells) as observed empirically using vascular-specific antibodies *in situ* (see Figure S7). No predilection for invasive glioma cells to migrate in association with arterials *versus* venules is observed. (B and C) Detailed views of invasive (B) and central (C) portions of perivascular brain tumors. White boxes shown in A correspond to the respective regions in B and C. (B) Illustration of brain perivascular potential space being infiltrated by invasive glioma cells. Adjacent microvessels have an average intervessel distance (AIVD) of ~50 μm (red scale bar), while the average tumor cell diameter (ACD) measures ~20 μm (green scale bar) as calculated empirically. Dashed white arrows represent the small intervening distance separating adjacent microvessels at the level of the capillary plexus. (C) Illustration of glioma cell division within the perivascular space. Glioma cell division within the perivascular space causes the displacement of normal brain tissue (i.e., neuropil, NP) between adjacent microvessels. The intervening space is then replaced by tumor cells while preexisting brain microvessels simultaneously become trapped within the growing tumor mass. Iterations of tumor cell invasion and division within the perivascular space causes further engulfment of preexisting brain microvessels, leading well-vascularized tumors early in tumor development through a neoangiogenesis-independent process we refer to as "autovascularization". (D) Details of the microanatomic arrangement at the tumor-vessel interface based on empirical observations.

microvessels may also be effective against perivascularly invading gliomas by eradicating preexistent brain microvessels already engulfed by perivascularly invading glioma cells. We conclude that malignant brain tumor autovascularization is a clinically relevant mechanism of VEGF-independent tumor vascularization whose therapeutic targeting is predicted to significantly impact clinical neurooncology.

Supplementary data to this article can be found online at http://dx.doi.org/10.1016/j.neo.2014.06.003.

Acknowledgments

We thank Roger Tsien (Department of Pharmacology, University of California San Diego) for kindly donating the pCI-neo-mCitrine expression vector. Plasmids encoding the Sleeping Beauty transposase/luciferase (pT2C-LucPGK-SB100X), shp53 (pT2-shp53-GFP4), and NRAS (pT2CAG-NRASV12) were generously provided by the laboratory of John Ohlfest (University of Minnesota). We gratefully acknowledge support for our work received from Philip Jenkins and the Department of Neurosurgery, University of Michigan School of Medicine. We are also grateful to Karin Muraszko for her academic leadership, M. Dahlgren, D. Tomford, and S. Napolitan for their superb administrative support, and Weidong Xiong for the generation of the GL26-Cit cell line. Author contributions: G.J.B, M.G.C., and P.R.L designed the research; G.J.B., V.N.Y, C.K., and Y.M. performed the research; S.M. designed and performed mathematical computations for the agent-based simulation; A.-A.C., S.B., W.S.N., A.C.D, T.M., S.I.C.-P, and D.O. contributed reagents and provided analytical tools; G.J.B., M.G.C., and P.R.L. analyzed the data; G.J.B., M.G.C., and P.R.L. wrote the paper. The authors declare no conflicts of interest.

References

[1] Dolecek TA, Propp JM, Stroup NE, and Kruchko C (2012). CBTRUS statistical report: primary brain and central nervous system tumors diagnosed in the United States in 2005–2009. *Neuro Oncol* **14**(Suppl 5), v1–v49.

[2] Grossman SA, Ye X, Piantadosi S, Desideri S, Nabors LB, Rosenfeld M, and Fisher J (2010). Survival of patients with newly diagnosed glioblastoma treated with radiation and temozolomide in research studies in the United States. *Clin Cancer Res* **16**, 2443–2449.

[3] Scherer HJ (1940). The forms of growth in gliomas and their practical significance. *Brain* **63**, 1–35.

[4] Scherer HJ (1938). Structural development in gliomas. *Am J Cancer* **34**, 333–351.

[5] Winkler F, Kienast Y, Fuhrmann M, Von Baumgarten L, Burgold S, Mitteregger G, Kretzschmar H, and Herms J (2009). Imaging glioma cell invasion in vivo reveals mechanisms of dissemination and peritumoral angiogenesis. *Glia* **57**, 1306–1315.

[6] Farin A, Suzuki SO, Weiker M, Goldman JE, Bruce JN, and Canoll P (2006). Transplanted glioma cells migrate and proliferate on host brain vasculature: a dynamic analysis. *Glia* **53**, 799–808.

[7] Holash J, Maisonpierre PC, Compton D, Boland P, Alexander CR, Zagzag D, Yancopoulos GD, and Wiegand SJ (1999). Vessel cooption, regression, and growth in tumors mediated by angiopoietins and VEGF. *Science* **284**, 1994–1998.

[8] Du R, Lu KV, Petritsch C, Liu P, Ganss R, Passegue E, Song H, Vandenberg S, Johnson RS, and Werb Z, et al (2008). HIF1α induces the recruitment of bone marrow-derived vascular modulatory cells to regulate tumor angiogenesis and invasion. *Cancer Cell* **13**, 206–220.

[9] Blouw B, Song H, Tihan T, Bosze J, Ferrara N, Gerber HP, Johnson RS, and Bergers G (2003). The hypoxic response of tumors is dependent on their microenvironment. *Cancer Cell* **4**, 133–146.

[10] Rubenstein JL, Kim J, Ozawa T, Zhang M, Westphal M, Deen DF, and Shuman MA (2000). Anti-VEGF antibody treatment of glioblastoma prolongs survival but results in increased vascular cooption. *Neoplasia* **2**, 306–314.

[11] Kunkel P, Ulbricht U, Bohlen P, Brockmann MA, Fillbrandt R, Stavrou D, Westphal M, and Lamszus K (2001). Inhibition of glioma angiogenesis and growth in vivo by systemic treatment with a monoclonal antibody against vascular endothelial growth factor receptor-2. *Cancer Res* **61**, 6624–6628.

[12] de Groot JF, Fuller G, Kumar AJ, Piao Y, Eterovic K, Ji Y, and Conrad CA (2010). Tumor invasion after treatment of glioblastoma with bevacizumab: radiographic and pathologic correlation in humans and mice. *Neuro Oncol* **12**, 233–242.

[13] Carbonell WS, DeLay M, Jahangiri A, Park CC, and Aghi MK (2013). β1 integrin targeting potentiates antiangiogenic therapy and inhibits the growth of bevacizumab-resistant glioblastoma. *Cancer Res* **73**, 3145–3154.

[14] Clark AJ, Lamborn KR, Butowski NA, Chang SM, Prados MD, Clarke JL, McDermott MW, Parsa AT, Berger MS, and Aghi MK (2012). Neurosurgical management and prognosis of patients with glioblastoma that progresses during bevacizumab treatment. *Neurosurgery* **70**, 361–370.

[15] Wiesner SM, Decker SA, Larson JD, Ericson K, Forster C, Gallardo JL, Long C, Demorest ZL, Zamora EA, and Low WC, et al (2009). De novo induction of genetically engineered brain tumors in mice using plasmid DNA. *Cancer Res* **69**, 431–439.

[16] Shaner NC, Steinbach PA, and Tsien RY (2005). A guide to choosing fluorescent proteins. *Nat Methods* **2**, 905–909.

[17] Constien R, Forde A, Liliensiek B, Grone HJ, Nawroth P, Hämmerling G, and Arnold B (2001). Characterization of a novel EGFP reporter mouse to monitor Cre recombination as demonstrated by a Tie2 Cre mouse line. *Genesis* **30**, 36–44.

[18] Motoike T, Loughna S, Perens E, Roman BL, Liao W, Chau TC, Richardson CD, Kawate T, Kuno J, and Weinstein BM, et al (2000). Universal GFP reporter for the study of vascular development. *Genesis* **28**, 75–81.

[19] Iliff JJ, Wang M, Liao Y, Plogg BA, Peng W, Gundersen GA, Benveniste H, Vates GE, Deane R, and Goldman SA, et al (2012). A paravascular pathway facilitates CSF flow through the brain parenchyma and the clearance of interstitial solutes, including amyloid β. *Sci Transl Med* **4**, 147ra111.

[20] Zhang ET, Richards HK, Kida S, and Weller RO (1992). Directional and compartmentalised drainage of interstitial fluid and cerebrospinal fluid from the rat brain. *Acta Neuropathol* **83**, 233–239.

[21] Pollock H, Hutchings M, Weller RO, and Zhang ET (1997). Perivascular spaces in the basal ganglia of the human brain: their relationship to lacunes. *J Anat* **191** (Pt 3), 337–346.

[22] Flanagan SP (1966). 'Nude', a new hairless gene with pleiotropic effects in the mouse. *Genet Res* **8**, 295–309.

[23] Binda E, Visioli A, Giani F, Lamorte G, Copetti M, Pitter KL, Huse JT, Cajola L, Zanetti N, and DiMeco F, et al (2012). The EphA2 receptor drives self-renewal and tumorigenicity in stem-like tumor-propagating cells from human glioblastomas. *Cancer Cell* **22**, 765–780.

[24] deCarvalho AC, Nelson K, Lemke N, Lehman NL, Arbab AS, Kalkanis S, and Mikkelsen T (2010). Gliosarcoma stem cells undergo glial and mesenchymal differentiation in vivo. *Stem Cells* **28**, 181–190.

[25] Carbonell WS, Ansorge O, Sibson N, and Muschel R (2009). The vascular basement membrane as "soil" in brain metastasis. *PLoS One* **4**, e5857.

[26] Fidler IJ, Yano S, Zhang RD, Fujimaki T, and Bucana CD (2002). The seed and soil hypothesis: vascularisation and brain metastases. *Lancet Oncol* **3**, 53–57.

[27] Camazine S (2001). Self-Organization in Biological Systems. Princeton, NJ: Princeton University Press; 2001 .

[28] Renshaw E and Henderson R (1981). The correlated random-walk. *J Appl Probab* **18**, 403–414.

[29] Kloeden PE and Platen E (1992). Numerical Solution of Stochastic Differential Equations. Berlin; New York: Springer-Verlag; 1992 .

[30] Ferrara N, Hillan KJ, Gerber HP, and Novotny W (2004). Discovery and development of bevacizumab, an anti-VEGF antibody for treating cancer. *Nat Rev Drug Discov* **3**, 391–400.

[31] Kienast Y, von Baumgarten L, Fuhrmann M, Klinkert WE, Goldbrunner R, Herms J, and Winkler F (2010). Real-time imaging reveals the single steps of brain metastasis formation. *Nat Med* **16**, 116–122.

[32] Jain RK (2005). Normalization of tumor vasculature: an emerging concept in antiangiogenic therapy. *Science* **307**, 58–62.

[33] Jain RK, di Tomaso E, Duda DG, Loeffler JS, Sorensen AG, and Batchelor TT (2007). Angiogenesis in brain tumours. *Nat Rev Neurosci* **8**, 610–622.

[34] Batchelor TT, Sorensen AG, di Tomaso E, Zhang WT, Duda DG, Cohen KS, Kozak KR, Cahill DP, Chen PJ, and Zhu M, et al (2007). AZD2171, a pan-

VEGF receptor tyrosine kinase inhibitor, normalizes tumor vasculature and alleviates edema in glioblastoma patients. *Cancer Cell* **11**, 83–95.

[35] Witte L, Hicklin DJ, Zhu Z, Pytowski B, Kotanides H, Rockwell P, and Böhlen P (1998). Monoclonal antibodies targeting the VEGF receptor-2 (Flk1/KDR) as an anti-angiogenic therapeutic strategy. *Cancer Metastasis Rev* **17**, 155–161.

[36] Jiang F, Zhang X, Kalkanis SN, Zhang Z, Yang H, Katakowski M, Hong X, Zheng X, Zhu Z, and Chopp M (2008). Combination therapy with antiangiogenic treatment and photodynamic therapy for the nude mouse bearing U87 glioblastoma. *Photochem Photobiol* **84**, 128–137.

[37] Martens T, Laabs Y, Günther HS, Kemming D, Zhu Z, Witte L, Hagel C, Westphal M, and Lamszus K (2008). Inhibition of glioblastoma growth in a highly invasive nude mouse model can be achieved by targeting epidermal growth factor receptor but not vascular endothelial growth factor receptor-2. *Clin Cancer Res* **14**, 5447–5458.

[38] King GD, Muhammad AK, Curtin JF, Barcia C, Puntel M, Liu C, Honig SB, Candolfi M, Mondkar S, and Lowenstein PR, et al (2008). Flt3L and TK gene therapy eradicate multifocal glioma in a syngeneic glioblastoma model. *Neuro Oncol* **10**, 19–31.

[39] King GD, Muhammad AG, Larocque D, Kelson KR, Xiong W, Liu C, Sanderson NS, Kroeger KM, Castro MG, and Lowenstein PR (2011). Combined Flt3L/TK gene therapy induces immunological surveillance which mediates an immune response against a surrogate brain tumor neoantigen. *Mol Ther* **19**, 1793–1801.

[40] Yu L, Wu X, Cheng Z, Lee CV, LeCouter J, Campa C, Fuh G, Lowman H, and Ferrara N (2008). Interaction between bevacizumab and murine VEGF-A: a reassessment. *Invest Ophthalmol Vis Sci* **49**, 522–527.

[41] Bock F, Onderka J, Dietrich T, Bachmann B, Kruse FE, Paschke M, Zahn G, and Cursiefen C (2007). Bevacizumab as a potent inhibitor of inflammatory corneal angiogenesis and lymphangiogenesis. *Invest Ophthalmol Vis Sci* **48**, 2545–2552.

[42] Hua J, Spee C, Kase S, Rennel ES, Magnussen AL, Qiu Y, Varey A, Dhayade S, Churchill AJ, and Harper SJ, et al (2010). Recombinant human VEGF165b inhibits experimental choroidal neovascularization. *Invest Ophthalmol Vis Sci* **51**, 4282–4288.

[43] Avisar I, Weinberger D, and Kremer I (2010). Effect of subconjunctival and intraocular bevacizumab injections on corneal neovascularization in a mouse model. *Curr Eye Res* **35**, 108–115.

[44] Folkman J (1971). Tumor angiogenesis: therapeutic implications. *N Engl J Med* **285**, 1182–1186.

[45] Folkman J and Hochberg M (1973). Self-regulation of growth in three dimensions. *J Exp Med* **138**, 745–753.

[46] Eberhard A, Kahlert S, Goede V, Hemmerlein B, Plate KH, and Augustin HG (2000). Heterogeneity of angiogenesis and blood vessel maturation in human tumors: implications for antiangiogenic tumor therapies. *Cancer Res* **60**, 1388–1393.

[47] Warburg O (1956). On the origin of cancer cells. *Science* **123**, 309–314.

[48] Flavahan WA, Wu Q, Hitomi M, Rahim N, Kim Y, Sloan AE, Weil RJ, Nakano I, Sarkaria JN, and Stringer BW, et al (2013). Brain tumor initiating cells adapt to restricted nutrition through preferential glucose uptake. *Nat Neurosci* **16**, 1373–1382.

[49] Wolfenson H, Lavelin I, and Geiger B (2013). Dynamic regulation of the structure and functions of integrin adhesions. *Dev Cell* **24**, 447–458.

[50] Presta LG, Chen H, O'Connor SJ, Chisholm V, Meng YG, Krummen L, Winkler M, and Ferrara N (1997). Humanization of an anti-vascular endothelial growth factor monoclonal antibody for the therapy of solid tumors and other disorders. *Cancer Res* **57**, 4593–4599.

[51] Wolburg H, Noell S, Fallier-Becker P, Mack AF, and Wolburg-Buchholz K (2012). The disturbed blood-brain barrier in human glioblastoma. *Mol Aspects Med* **33**, 579–589.

[52] Huveldt D, Lewis-Tuffin LJ, Carlson BL, Schroeder MA, Rodriguez F, Giannini C, Galanis E, Sarkaria JN, and Anastasiadis PZ (2013). Targeting Src family kinases inhibits bevacizumab-induced glioma cell invasion. *PLoS One* **8**, e56505.

[53] Gilbert MR, Dignam JJ, Armstrong TS, Wefel JS, Blumenthal DT, Vogelbaum MA, Colman H, Chakravarti A, Pugh S, and Won M, et al (2014). A randomized trial of bevacizumab for newly diagnosed glioblastoma. *N Engl J Med* **370**, 699–708.

[54] Chinot OL, Wick W, Mason W, Henriksson R, Saran F, Nishikawa R, Carpentier AF, Hoang-Xuan K, Kavan P, and Cernea D, et al (2014). Bevacizumab plus radiotherapy-temozolomide for newly diagnosed glioblastoma. *N Engl J Med* **370**, 709–722.

[55] Lucio-Eterovic AK, Piao Y, and de Groot JF (2009). Mediators of glioblastoma resistance and invasion during antivascular endothelial growth factor therapy. *Clin Cancer Res* **15**, 4589–4599.

[56] Candolfi M, Curtin JF, Nichols WS, Muhammad AG, King GD, Pluhar GE, McNiel EA, Ohlfest JR, Freese AB, and Moore PF, et al (2007). Intracranial glioblastoma models in preclinical neuro-oncology: neuropathological characterization and tumor progression. *J Neurooncol* **85**, 133–148.